

FOURIER ANALYSIS OF DE HAAS-VAN ALPHEN
EFFECT DATA

FOURIER ANALYSIS OF DE HAAS-VAN ALPHEN
EFFECT DATA

By

JOHN CONRAD JONES, B.A.

A Thesis

Submitted to the Faculty of Graduate Studies
in Partial Fulfilment of the Requirements
for the Degree
Master of Science

McMaster University

April 1968

MASTER OF SCIENCE
(Physics)

McMASTER UNIVERSITY
Hamilton, Ontario

TITLE: Fourier Analysis of de Haas-van Alphen Effect Data

AUTHOR: John Conrad Jones, B.A. (Oxford University)

SUPERVISOR: Professor W. R. Datars

NUMBER OF PAGES: vii, 64

SCOPE AND CONTENTS:

A digital program has been developed to Fourier analyse the data obtained in experiments to study the de Haas-van Alphen effect. A physical account of the origin of this effect is given and the problem of analysing the data is explained. An account is given of the development of the program together with a consideration of the mathematical properties of the Fourier transform. General questions concerning the resolving power and accuracy of this method of analysis are discussed. The program was tested using artificial synthetic data of known analytic form and later applied to the analysis of data from a single crystal of mercury.

ACKNOWLEDGEMENTS

The author wishes to thank Professor W. R. Datars for his guidance and help throughout the course of this research.

I also wish to thank Mr. John Vanderkooy and Mr. John S. Moss for many valuable discussions during the course of this work.

Financial aid was received from McMaster University and the National Research Council of Canada, to whom the author is greatly indebted.

TABLE OF CONTENTS

<u>CHAPTER</u>	<u>SUBJECT</u>	<u>PAGE</u>
	INTRODUCTION	1
I	THE INFLUENCE OF A STEADY MAGNETIC FIELD ON THE CONDUCTION ELECTRONS IN A CRYSTAL	5
II	DATA ANALYSIS BY FOURIER TRANSFORM	21
III	DEVELOPMENT OF THE DIGITAL PROGRAM	38
IV	TESTING PROGRAM USING ARTIFICIAL DATA	50
V	APPLICATION OF THE PROGRAM TO REAL DATA	58
	BIBLIOGRAPHY	64

LIST OF ILLUSTRATIONS

<u>FIGURE</u>	<u>SUBJECT</u>	<u>PAGE</u>
II.1	Rectangular window function	33
II.2	Exponential window function	33
II.3	Cosine window function	33
IV.1	Graph of function used as artificial data	53
IV.2	Fourier analysis of this function using rectangular, cosine and Gaussian window functions	54
IV.3	Fourier analysis of this function using rectangular, cosine and Gaussian window functions	55
IV.4	Fourier analysis of this function using rectangular, cosine and Gaussian window functions	56
V.1	Experimental trace and Fourier analysis of de Haas-van Alphen effect data for a single crystal of mercury with magnetic field orientation close to the trigonal-bisectrix plane.	61
V.2	Experimental trace and Fourier analysis of de Haas-van Alphen effect data for a single crystal of mercury with magnetic field orientation close to the trigonal-bisectrix plane.	62
V.3	Experimental trace and Fourier analysis of de Haas-van Alphen effect data for a single	63

LIST OF ILLUSTRATIONS (CONTINUED)

crystal of mercury with magnetic field
orientation close to the trigonal-bisectrix
plane

LIST OF TABLES

<u>TABLE</u>	<u>SUBJECT</u>	<u>PAGE</u>
IV.1	Tabulated values of frequencies ω and relative amplitudes A of the Fourier transform of the function used as artificial data	57

INTRODUCTION

The de Haas-van Alphen effect is an oscillatory variation of the magnetic susceptibility periodic in $1/H$ which is observed in metals at low temperatures when the magnetic field is varied.

It was first observed in 1930 by W. J. de Haas and P. M. van Alphen¹ in the course of measurements on the magnetic susceptibility of bismuth single crystals. It has since been observed in many metals and semi-metals and the effect has provided one of the most powerful tools for the experimental determination of the topology of Fermi surfaces. Landau in a paper on the theory of diamagnetism of metals², also published in 1930, predicted the oscillatory field variation of susceptibility before he knew of de Haas and van Alphen's experiments but believed that in practice field inhomogeneities would render the effect unobservable because of phase cancellations between the oscillations coming from regions of the crystal at slightly different fields. Peierls³ laid the foundation of the theory of the effect by showing that the magnetization of a free electron gas should oscillate as the field is varied because of the quantization

of the free electron orbits in a magnetic field.

A most important theoretical advance was made by Onsager⁴ in 1952 who showed that the period of the oscillations is inversely proportional to the extreme area of cross section of the Fermi surface by planes normal to the field.

Lifshitz and Kosevich⁵ have developed a comprehensive theory which embraces Onsager's main result and provides a comprehensive formula to describe the effect. It frequently happens that there are several extremal areas of cross section of Fermi surface perpendicular to a particular field direction. This occurs especially in the polyvalent metals where there are small isolated pieces of Fermi surface symmetrically distributed in reciprocal space arising from pockets of holes at the corners of incompletely filled Brillouin zones and from small pockets of electrons overlapping across Brillouin zone faces. Thus the de Haas-van Alphen oscillations are quite complicated in some materials at some field orientations, because the observed oscillation is really a superposition of several oscillations differing in frequency, amplitude and phase. Therefore it becomes a major problem to analyze the various component oscillations.

One way of analyzing a complex waveform is to

resort to a Fourier transformation. A digital program to compute the Fourier transform of de Haas-van Alphen effect data has been developed. An account will be given of the development of this program, and of its properties and applications.

The first chapter of this thesis will be a consideration of the properties of conduction electrons in a magnetic field, with an outline of the theory of the de Haas-van Alphen effect. The rather complicated analytical expression of Lifshitz and Kosevich will be reduced to a simpler approximate form.

In the second chapter the simplified approximate formula will be considered, and it will be shown that the Fourier spectrum of the de Haas-van Alphen effect data will exhibit peaks at, or very near, the frequencies of the component oscillations in the data. The questions of resolving power, displacement of the Fourier spectrum peaks under some conditions, noise, sidebands and the suppression of sidebands will be discussed.

In Chapter three the digital program is described, a description of the mathematical procedures used in computing the Fourier spectrum of the data is given, together with an account of some precautions that are taken to prevent serious errors from occurring at especially sensitive points in the calculation.

Chapter IV is an account of numerical experiments that were performed, in which the program analyses ideal synthetic data of known analytic form, thus validating the program.

In Chapter V a brief account is given of the application of the program to real data. It has been used in the analysis of data from mercury and ytterbium crystals.

CHAPTER I

THE INFLUENCE OF A STEADY MAGNETIC FIELD ON THE CONDUCTION ELECTRONS IN A CRYSTAL

Using the single electron approximation the Schrödinger equation of the system is

$$\left\{ \frac{1}{2m} \left(\frac{\hbar}{i} \nabla - \frac{e}{c} \underline{A} \right)^2 + V(\underline{r}) \right\} \psi(\underline{r}) = \epsilon \psi(\underline{r}) \quad (1)$$

where \underline{A} is the magnetic vector potential. If there is a uniform field \underline{H} in the z direction then $\underline{A} = (0, Hx, 0)$ in the Landau gauge. \underline{A} does not have the translational symmetry of the lattice and Bloch's theorem does not apply in the presence of a magnetic field.

To understand the motion in \underline{k} space consider the semi-classical equation of motion.

$$\dot{\underline{k}} = \frac{e}{c\hbar} \underline{v} \times \underline{H} . \quad (2)$$

This means that the change in the vector \underline{k} is

- (i) normal to the direction of \underline{H}
- (ii) normal to \underline{v} which is itself normal to the equipotentials of constant energy in \underline{k} space.
- (iii) \underline{k} moves along a curve of constant energy because electrons cannot pick up energy from a static magnetic field.

Each electron is to be imagined moving along a curve

of constant energy in a plane normal to \underline{H} . If the electron is not scattered it makes a circuit in the period

$$\frac{2\pi}{\omega_H} = \frac{c\hbar}{eH} \oint \frac{dk_{\perp}}{V_{\perp}}, \quad (3)$$

where V_{\perp} is the component of \underline{V} in the plane normal to \underline{H} at the point \underline{k} , and ω_H is called the cyclotron frequency. This frequency may be written as $\frac{eH}{m_H^*}$ where m_H^* is called the cyclotron mass. A geometrical $m_H^* C$ definition of m_H^* can be given using the relationship $V_{\perp} = \frac{1}{\hbar} \frac{d\mathcal{E}}{dk_{\perp}}$ where dk_{\perp} is an increment of k in the plane of the orbit normal to the equipotential curve:

$$m_H^* = \frac{\hbar^2}{2\pi} \oint \frac{dk_{\perp}}{d\mathcal{E}} dk = \frac{\hbar^2}{2\pi} \frac{\partial \mathcal{A}}{\partial \mathcal{E}} \quad (4)$$

where \mathcal{A} is the area enclosed by the orbit in the plane normal to \underline{H} .

Another useful orbit parameter is the phase variable

$$\phi \text{ defined by } \phi = \omega_H \frac{c\hbar}{eH} \int^k \frac{dk_{\perp}}{V_{\perp}}. \quad (5)$$

ϕ increases at a constant rate, $\dot{\phi} = \omega_H$ and $\phi = 2\pi$ for a complete circuit.

The details of the electron's motion in \underline{r} space can be deduced from equation (2). The general solution of this equation is

$$\underline{k} = \frac{e}{c\hbar} \{ \underline{r} + f(t)\underline{H} \} \times \underline{H} + \underline{b}, \quad (6)$$

where \underline{b} is an arbitrary constant vector and $f(t)$ is an arbitrary function of the time. If vectors are expressed in

terms of components parallel to \underline{H} and perpendicular to \underline{H} , equation (6) becomes

$$\underline{k}_H + \underline{k}_\perp = \frac{e}{c\hbar} \{ \underline{r}_H + \underline{r}_\perp + f(t)\underline{H} \} \times \underline{H} + \underline{b}_H + \underline{b}_\perp .$$

$$\underline{k}_H + \underline{k}_\perp = \frac{e}{c\hbar} \underline{r}_\perp \times \underline{H} + \underline{b}_H + \underline{b}_\perp$$

Therefore

$$\underline{k}_\perp = \frac{e}{c\hbar} \underline{r}_\perp \times \underline{H} + \underline{b}_\perp . \quad (7)$$

Equation (7) establishes Onsager's theorem that the projection of the electron's orbit in real space on to a plane perpendicular to \underline{H} is geometrically similar to the \underline{k} space orbit but is rotated through $\frac{\pi}{2}$ radians around \underline{H} and is scaled by a factor $c\hbar/eH$.

The electron orbit in real space is a helix with its axis parallel to \underline{H} . The helix may be complex in form and even when it is a closed curve forming a stationary orbit in \underline{r} space it will not necessarily be a plane curve, it may be a buckled irregular ring, or it may be tilted with respect to \underline{H} . The net displacement of the electron after it has completed a revolution about the helix axis is called the pitch of the helix.

The deduction of a formula for the pitch of the helix.

Consider an electron going around its orbit in \underline{k} space. Setting up the phase variable ϕ as in equation (5),

$\phi = \text{constant}$, and ϕ increases by 2π around the orbit.

$$\phi = \omega_H t = \frac{eH}{m_H^* c} t = \frac{eH(2\pi)}{\hbar^2 c \left(\frac{\partial A}{\partial \epsilon}\right)} t$$

$$dt = \hbar^2 c \left(\frac{\partial A}{\partial \epsilon}\right) \frac{1}{2\pi eH} d\phi$$

$$\text{Now } \underline{\dot{k}} = \frac{e}{c\hbar} \underline{v} \times \underline{H} = \frac{e}{c\hbar^2} (\nabla_{\underline{k}} \epsilon) \times \underline{H},$$

therefore the electron velocity around the orbit is

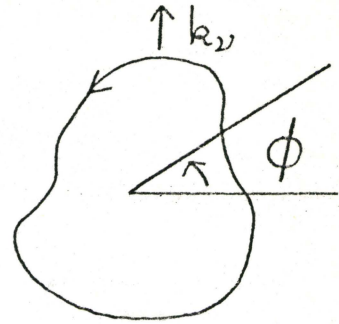
$\underline{v}_{\underline{k}} = \frac{eH}{c\hbar^2} \frac{\partial \epsilon}{\partial k_{\nu}}$ where \underline{k}_{ν} lies in the plane of the orbit and is normal to the orbit at any point. Thus the distance dS travelled by the electron when the phase variable increases by $d\phi$ is given by

$$d_S = v_K dt = \frac{eH}{c\hbar^2} \frac{\partial \epsilon}{\partial k_{\nu}} \times \hbar^2 c \left(\frac{\partial A}{\partial \epsilon}\right) \frac{1}{2\pi eH} d\phi$$

$$d_S = \frac{1}{2\pi} \left(\frac{\partial A}{\partial k_{\nu}}\right) d\phi. \quad (8)$$

If the magnetic field \underline{H} is in the z direction, the electron orbit in \underline{k} space will lie in a plane k_{z0} perpendicular to the z axis.

On the orbit considered imagine the ϕ variable increasing from 0 to 2π . Through all the equipotential surfaces in the plane k_{z0} draw curves orthogonal to them which are given coordinates which coincide with the value of the phase variable ϕ on the orbit under consideration. Any point in the plane k_{z0} can now be specified by the coordinates $\{A, \phi\}$ where A is the cross sectional area of



the equipotential curve on which the point lies. The coordinate ϕ coincides with the phase variable on the special orbit under consideration but does not necessarily do so on the other equipotential curves in the plane.

Produce the equipotential curves in the plane k_{z0} in the z direction forming a set of cylinders. By construction these cylinders coincide with the true equipotentials only in the plane k_{z0} but not necessarily so elsewhere. We now have an orthogonal coordinate system (\mathcal{A}, ϕ, k_z) to describe any point in \underline{k} space. Another coordinate system (A, ϕ, k_z) can be set up where k_z, ϕ are defined as before, but A is the true area of the cross section in the plane k_z of the equipotential on which the point under consideration lies. By construction \mathcal{A} coincides with A in the plane k_{z0} .

The pitch of the real space helix for the orbit under consideration is given by

$$\begin{aligned}
 \text{Pitch} &= \frac{1}{\hbar} \int \left(\frac{\partial \epsilon}{\partial k_z} \right) \mathcal{A}, \phi \, dt \\
 &= \frac{1}{\hbar} \int \left(\frac{\partial \epsilon}{\partial k_z} \right) \mathcal{A}, \phi \frac{\hbar^2 c}{2\pi e H} \left(\frac{\partial \mathcal{A}}{\partial \epsilon} \right)_{k_0} d\phi \\
 &= \frac{\hbar c}{2\pi e H} \left(\frac{\partial \mathcal{A}}{\partial \epsilon} \right)_{k_0} \int \left(\frac{\partial \epsilon}{\partial k_z} \right) \mathcal{A}, \phi \, d\phi \quad (9)
 \end{aligned}$$

where $\left(\frac{\partial \mathcal{A}}{\partial \epsilon} \right)_{k_0}$ relates to the special orbit being considered.

But $\epsilon = \epsilon\{\mathcal{A}, k_z, \phi\}$

so that $d\epsilon = \left(\frac{\partial \epsilon}{\partial \mathcal{A}} \right)_{k_z, \phi} d\mathcal{A} + \left(\frac{\partial \epsilon}{\partial k_z} \right) \mathcal{A}, \phi \, dk_z + \left(\frac{\partial \epsilon}{\partial \phi} \right) \mathcal{A}, k_z \, d\phi$

but $\mathcal{A} = \mathcal{A}\{\varepsilon, k_z, \varnothing\}$,

$$\text{therefore } \left(\frac{\partial \varepsilon}{\partial k_z}\right)_{\mathcal{A}, \varnothing} = - \left(\frac{\partial \varepsilon}{\partial \mathcal{A}}\right)_{k_z, \varnothing} \left(\frac{\partial \mathcal{A}}{\partial k_z}\right)_{\varepsilon, \varnothing} . \quad (10)$$

In the plane k_{z0} $\left(\frac{\partial \varepsilon}{\partial \mathcal{A}}\right)$ is independent of \varnothing , substituting from equation (10) in equation (9).

$$\begin{aligned} \text{Pitch} &= - \frac{\hbar c}{2\pi e H} \left(\frac{\partial \mathcal{A}}{\partial \varepsilon}\right)_{k_z, \varnothing} \left(\frac{\partial \varepsilon}{\partial \mathcal{A}}\right)_{k_z, \varnothing} \left\{ \left(\frac{\partial \mathcal{A}}{\partial k_z}\right)_{\varepsilon, \varnothing} d\varnothing \right. \\ &\quad \left. \text{Pitch} = - \frac{\hbar c}{2\pi e H} \left\{ \left(\frac{\partial \mathcal{A}}{\partial k_z}\right)_{\varepsilon, \varnothing} d\varnothing \right. \right. \end{aligned} \quad (11)$$

But $\mathcal{A} = \mathcal{A}\{A, k_z, \varnothing\}$

therefore

$$d\mathcal{A} = \left(\frac{\partial \mathcal{A}}{\partial A}\right)_{k_z, \varnothing} dA + \left(\frac{\partial \mathcal{A}}{\partial k_z}\right)_{A, \varnothing} dk_z + \left(\frac{\partial \mathcal{A}}{\partial \varnothing}\right)_{A, k_z} d\varnothing .$$

However

$$A = A\{\varepsilon, k_z, \varnothing\}$$

giving

$$\begin{aligned} d\mathcal{A} &= \left(\frac{\partial \mathcal{A}}{\partial A}\right)_{k_z, \varnothing} \left\{ \left(\frac{\partial A}{\partial \varepsilon}\right)_{k_z, \varnothing} d\varepsilon + \left(\frac{\partial A}{\partial k_z}\right)_{\varepsilon, \varnothing} dk_z \right. \\ &\quad \left. + \left(\frac{\partial A}{\partial \varnothing}\right)_{\varepsilon, k_z} d\varnothing \right\} + \left(\frac{\partial \mathcal{A}}{\partial k_z}\right)_{A, \varnothing} dk_z + \left(\frac{\partial \mathcal{A}}{\partial \varnothing}\right)_{A, k_z} d\varnothing . \end{aligned}$$

Therefore

$$\left(\frac{\partial \mathcal{A}}{\partial k_z}\right)_{\varepsilon, \varnothing} = \left(\frac{\partial \mathcal{A}}{\partial A}\right)_{k_z, \varnothing} \left(\frac{\partial A}{\partial k_z}\right)_{\varepsilon, \varnothing} + \left(\frac{\partial \mathcal{A}}{\partial k_z}\right)_{A, \varnothing}$$

but A is really a function of ε and k_z alone with \varnothing as an ignorable coordinate. In the plane k_{z0} $\mathcal{A} \equiv A$ so that

$$\left(\frac{\partial A}{\partial k_z}\right)_{k_{z0}, \phi} = 1.$$

Therefore

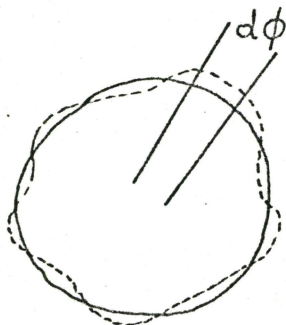
$$\left(\frac{\partial A}{\partial k_z}\right)_{\epsilon, \phi} = \left(\frac{\partial A}{\partial k_z}\right)_{\epsilon} + \left(\frac{\partial A}{\partial k_z}\right)_{A, \phi},$$

so that

$$\text{Pitch} = -\frac{\hbar c}{2\pi eH} \int \left[\left(\frac{\partial A}{\partial k_z}\right)_{\epsilon} + \left(\frac{\partial A}{\partial k_z}\right)_{A, \phi} \right] d\phi,$$

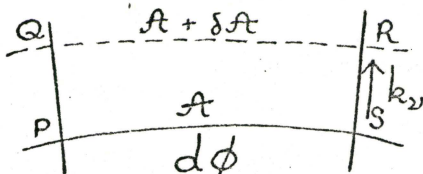
$$\text{Pitch} = -\frac{\hbar c}{eH} \left(\frac{\partial A}{\partial k_z}\right)_{\epsilon} - \frac{\hbar c}{2\pi eH} \int \left(\frac{\partial A}{\partial k_z}\right)_{A, \phi} d\phi.$$

To prove the last integral to be zero consider the orbit of Area A in plane $k_{z0} + dk_z$ which has the same area as the orbit under consideration. In the diagram



the dotted curve represents the orbit in the plane $k_{z0} + dk_z$, the full curve represents the special orbit being considered. The two curves are equal in area.

Projecting the dotted curve on to the plane k_{z0} and considering a short section of both curves along an arc $d\phi$.



Let QR be centred on the $A + dA$ cylinder, $PQRS$ is a rectangle if $d\phi$ is small enough, dk_z is assumed arbitrarily small.

The area of the rectangle equals $PQ \times PS$.

$$PQ = \left(\frac{\delta k_v}{\delta A} \right) \delta A = \left(\frac{\delta k_v}{\delta A} \right) \left(\frac{\partial A}{\partial k_z} \right)_{A, \phi} dk_z ,$$

$$PS = \frac{1}{2\pi} \left(\frac{\delta A}{\delta k_v} \right) d\phi$$

using equation (8). Therefore area of rectangle =

$$\begin{aligned} & \frac{1}{2\pi} \left(\frac{\delta A}{\delta k_v} \right) d\phi \left(\frac{\delta k_v}{\delta A} \right) \left(\frac{\partial A}{\partial k_z} \right)_{\phi, A} dk_z \\ & = \frac{1}{2\pi} dk_z d\phi \left(\frac{\partial A}{\partial k_z} \right)_{A, \phi} . \end{aligned}$$

The difference in area of the two orbits is equal to

$$\frac{1}{2\pi} (dk_z) \oint \left(\frac{\partial A}{\partial k_z} \right)_{A, \phi} d\phi ,$$

but the two areas are equal by definition. Therefore

$$\oint \left(\frac{\partial A}{\partial k_z} \right)_{A, \phi} d\phi = 0 .$$

This means that equation (12) reduces to

$$\text{Pitch} = - \frac{\hbar c}{eH} \left(\frac{\partial A}{\partial k_z} \right)_{\epsilon}$$

and the necessary and sufficient condition for an orbit to be stationary in real space is that in \underline{k} space it be an extremum of area for the particular orientation of the magnetic field. But these extremum orbits on the Fermi surface turn out to be exactly those which produce the most significant contribution to the de Haas-van Alphen effect.

The theorem which has been proved shows that these orbits are also stationary in real space.

Magnetic Quantization

The projection of the electronic motion on to a plane perpendicular to \underline{H} forms a closed curve and the Bohr-Sommerfeld phase integral formula can be applied:

$$\oint \underline{p}_{\perp} \cdot d\underline{r}_{\perp} = (n+\gamma)h \quad (13)$$

where n is an integer and γ is a constant which has been added to n to make the theory physically more reasonable. For example the Bohr-Sommerfeld theory predicts the harmonic oscillator energy levels to be $E_n = n\hbar\omega$, whereas in fact $E_n = (n + \frac{1}{2})\hbar\omega$. Roth⁶ and R. G. Chambers⁶ have shown that γ is always $\frac{1}{2}$ in weak fields and Roth⁷ has shown that when ω_H is a function of energy, γ is of the form

$$\gamma = \frac{1}{2} + \gamma_1 |H| + \dots$$

Substituting into equation (13) using the relationship

$$\underline{p} = \hbar\underline{k} + \frac{e}{c} \underline{A},$$

where $\underline{A} = H(0, x, 0)$ in the Landau gauge.

Resolving vectors perpendicular to \underline{H} ,

$$\underline{A}_{\perp} = \underline{A}, \quad \underline{p}_{\perp} = \hbar\underline{k}_{\perp} + \frac{e}{c} \underline{A}.$$

Therefore

$$\oint \underline{p}_{\perp} \cdot d\underline{r}_{\perp} = \oint (\hbar\underline{k}_{\perp} + \frac{e}{c} \underline{A}) \cdot d\underline{r}_{\perp},$$

but from Onsager's theorem

$$\underline{k}_{\perp} = \frac{e}{ch} \underline{r}_{\perp} \times \underline{H} + \underline{b}_{\perp} .$$

The arbitrary constant \underline{b}_{\perp} can be neglected because it integrates out to give zero.

Substituting into the phase integral

$$\oint \underline{p}_{\perp} \cdot d\underline{r}_{\perp} = \oint \left(-\frac{\hbar e}{ch} \underline{H} \times \underline{r}_{\perp} + \frac{e}{c} \underline{A} \right) \cdot d\underline{r}_{\perp} = (n+\gamma)h$$

which can be transformed to give

$$-\frac{e}{c} \oint \underline{H} \cdot (\underline{r}_{\perp} \times d\underline{r}_{\perp}) + \frac{e}{c} \int \nabla \times \underline{A} \cdot d\underline{A}_r = (n+\gamma)h$$

where A_r is the area of the projection of the real space orbit on to a plane perpendicular to \underline{H} . Thus we obtain the result

$$-\frac{e}{c} H A_r = (n+\gamma)h .$$

Therefore the possible values of A_r are given by

$$A_r = (n+\gamma) \left(\frac{ch}{e} \right) \frac{1}{H} , \quad n = 0, 1, 2, \dots .$$

A physically more fundamental result follows from

$$HA_r = (n+\gamma) \left(\frac{ch}{e} \right) ,$$

the flux enclosed by an orbiting electron helix is quantized in units of $\left(\frac{hc}{e} \right)$. Using equation (7), Onsager's theorem, A_K the cross sectional area of the orbit in \underline{k} space is given by

$$A_K = \left(\frac{eH}{ch} \right)^2 A_r .$$

Therefore

$$A_K = 2\pi(n+\gamma) \frac{eH}{c\hbar} .$$

The description of the electron energy levels in a magnetic field requires the following construction in \underline{k} space. Choose a value of n , on each plane of section of the Fermi surface normal to the magnetic field draw the energy contour of area A_n . Join these contours into a continuous tube with constant area of cross section, draw similar tubes for other values of n . By rigorously solving the Schrödinger equation in the magnetic field it can be shown that the degeneracy of these Landau levels is the same as would occur if all the allowed points in the usual Bloch scheme condensed on to the nearest tube. By the correspondence principle the energy difference between successive Landau levels should be $\hbar\omega_H$. In the free electron case it has been shown rigorously that $\epsilon(n+\gamma, k_z) = (n+\gamma)\hbar\omega_H + f(k_z)$. A rigorous proof in the general case has never been given.

Physical consequences of the magnetic quantization

As the magnetic field gradually increases the tubes of magnetic quantization expand and one by one they break through the Fermi surface with a frequency that is proportional to $1/H$, consequently any physical parameter of the system should possess a component periodic in $1/H$. The oscillations in the magnetic susceptibility constitute the de Haas-van Alphen effects, a similar oscillation in the

electrical conductivity is called the de Haas-Shubnikov effect.

To understand how the de Haas-van Alphen effect arises it is customary to consider the thermodynamic free energy. For a Fermi-Dirac assembly this is given by

$$F = N\zeta - kT \sum_i \ln(1 + \exp(\zeta - \epsilon_i)/kT) \quad (14)$$

where the summation is over all possible states, ζ is the Fermi potential. It is clear that as the Landau levels expand the most significant variations in F arise from the regions near the extremal orbits in \underline{k} space for which $\frac{\partial A_k}{\partial k_z} = 0$. As the Landau levels break through the Fermi surface near an extremal orbit F should have an oscillatory variation whose amplitude is determined in some way by the curvature of the Fermi surface around the extremal area.

It has been shown by Lifshitz and Kosevich that for a general shape of Fermi surface the oscillatory part of F can be given by the rather complicated expression

$$F = 2kT \left(\frac{e}{ch}\right)^{3/2} |A_0''|^{-1/2} H^{3/2} \sum_{s=1}^{\infty} \frac{(-1)^s}{s^{3/2}} \frac{\cos\left(\frac{sch}{eH} A_0 \pm \frac{\pi}{4}\right) \cos\left(\frac{\pi m_H^*}{m_0}\right)}{\sinh\left(\frac{2\pi^2 s k (T+T_D)}{h\omega_H}\right)} \quad (15)$$

The above expression gives the oscillations in F arising from a particular extremal area for which $A = A_0 \pm \frac{1}{2} k_z^2 A_0''$, it is seen that the oscillations are periodic in $1/H$ with a period $P = \frac{2\pi e}{Sch A_0''}$ and an amplitude partly governed by the curvature term $|A_0''|^{-1/2}$. If there are several extremal areas

then each one will contribute a term like equation (15) to the resultant variation in F which will therefore be a superposition of oscillations of differing frequencies periodic in $1/H$. The \pm signs apply in equation (15) according to whether A represents a maximum (-) or a minimum (+).

Another factor determining the amplitude of the oscillations is the temperature. If the temperature is 0°K and the Fermi surface is perfectly sharp and we suppose that the field is such that ζ lies halfway between two Landau levels, then the number of states below the Fermi level will be the same as if there were no magnetic levels, but the total energy of the electron gas will be less than in the absence of a magnetic field by about $\frac{1}{2} \hbar \omega_H$ per electron at the Fermi level. As H increases these electrons will be drawn up to the Fermi level so their free energy increases to a maximum, but when a magnetic level passes through the Fermi level it begins to empty and the energy drops again reaching a minimum when the Fermi level lies halfway between two quantized levels again. If the Fermi surface is not infinitely sharp and is thermally broadened because of the temperature of the electron gas, then at $T^\circ\text{K}$ the energy width of the Fermi surface is approximately kT . If the temperature is such that several magnetic levels are contained in this narrow region of width kT the variation

of the electron gas energy will be much smoother than at 0°K and if $kT \gg \hbar\omega_H$ no oscillations will be observed at all. This essentially is why the de Haas-van Alphen effect is a low temperature phenomenon and why the amplitude of the oscillations decreases with increasing temperature.

The last cosine factor in equation (15) comes from the doubling of the energy levels on account of the magnetic moment of the electron spin. Electrons of opposite spin condense on to different sets of Landau levels and the oscillations arising from the two sets of levels may differ in phase, it is even possible for no oscillations to be observed at all because of interference between the sets of levels. The form $\text{Cos}\left(\frac{\pi m_H^*}{m_0}\right)$, where m_0 is the free electron mass was first given by Dingle⁸. This factor is often nearly unity because m_H is usually much less than m_0 .

The amplitude of the oscillations is reduced if account is taken of a possible broadening of the line-width of the energy levels due to collisions or other causes. Dingle⁹ showed that on certain simplifying assumptions the effect of the broadening that would correspond to a collision time τ is as if the temperature T is replaced by $(T+T_D)$ in the sinh term of equation (15) where $T_D = \frac{\hbar}{2\pi^2 k\tau}$, T_D is called the Dingle temperature. From equation (15) it is possible to obtain either M , the magnetization = $-\frac{\partial F}{\partial H}$, or C the couple about any axis = $-\frac{\partial F}{\partial \psi}$, where ψ is an angle speci-

ying rotation in a plane normal to the axis. In the differentiations the main contributions come only from differentiation of the cosine term because $\frac{chA_0}{eH} \gg 1$. Thus the simplified expressions for M and C will differ from (15)

only by a change from Cos to Sin and an extra factor $\frac{schA_0}{EH^2}$ for M and $(-\frac{sch}{eH} \frac{\partial A_0}{\partial \psi})$ in C.

It is important to note that if a torque magnetometer is used in observations of the de Haas-van Alphen effect, zero torque may be observed because for the particular orientation chosen $\frac{\partial A_0}{\partial \psi} = 0$, the torque method has a blind spot. For this reason the torque magnetometer would not be very useful in experiments on the alkali metals where the Fermi surfaces are very nearly spherical.

Because $\hbar\omega_H = \hbar(\frac{eH}{m_H^* c})$, the terms $\sinh(\frac{2\pi^2 kTs}{h\omega_H})$ can be written as $(\sinh(\frac{s\lambda}{H}))$ where $\lambda = \frac{2\pi^2 m_H^* c}{he} (kT)$. If $\frac{\lambda}{H}$ is substantially greater than unity we can approximate $\sinh(\frac{\lambda}{H}) \approx \exp(\frac{\lambda}{H})$ and taking only the first term in equation (15)

$$F \approx 2kT \left(\frac{eH}{2\pi ch}\right)^{3/2} |A_0|^{-1/2} e^{-\frac{\lambda}{H}} \cos\left(\frac{chA_0}{eH} \pm \frac{\pi}{4}\right).$$

In this approximation the de Haas-van Alphen oscillations are a periodic function in $\frac{1}{H}$ with a period $P = \frac{2\pi e}{chA_0}$ and an amplitude that increases with increasing field because of the exponential factor. If P can be determined, then the extremal area of cross section of the Fermi surface is obtained directly. At higher fields and lower temperatures

the high order terms in equation (15) corresponding to $s = 2, 3, 4$, etc. cannot be neglected. Consequently the oscillations become richer in higher frequency harmonics. Another factor contributing to the existence of higher harmonics is a skewness introduced into the oscillations due to the fact that the true field seen by the electrons is \underline{B} not \underline{H} . This causes the cosine waves to be steeper on one side than on the other. Consequently the general form of the oscillation to be analyzed is

$$C = \sum_i A_i \exp\left(-\frac{\lambda_i}{H}\right) \sin\left(\frac{\omega_i}{H} + \alpha_i\right) . \quad (16)$$

Actual experimental data are often too complicated to be analyzed easily, particularly when there are many terms in equation (16).

CHAPTER II

DATA ANALYSIS BY FOURIER TRANSFORM

Equation (16) can be written

$$Y = \sum_i A_i \exp(-\lambda_i x) \sin(\omega_i x + \alpha_i),$$

where

$$x = \frac{1}{H}. \quad (17)$$

If a Fourier transformation of the data is carried out for a range of values of ω , the amplitude function $A(\omega)$ of the Fourier transform should show peaks in the neighbourhood of the frequencies ω_i . In this way the frequency spectrum of the data would be obtained and the problem of analyzing the data would be resolved.

However, there are a number of complicating factors that raise a variety of questions. Any experimental record is of finite length, this truncation introduces a broadening of the amplitude peaks in the Fourier transform and introduces sidebands around the main peaks. This brings in the question of resolving power and the problem of separating true peaks from sidebands. Another factor is the existence of the exponential terms $\exp(-\lambda_i x)$ which would also be expected to have a broadening effect on the peaks, much as the spectrum of a damped harmonic oscillator gives a Lorentzian line shape. The exponential terms might also be suspected of causing the amplitude peaks to shift by a small

amount from the frequencies ω_i that are really of interest. The distortions of the sinusoidal wave form by the truncation and the exponential factors might be expected to introduce artificial harmonics of the frequencies ω_i .

It can be shown that peak shifting due to the exponential factors is entirely negligible and that spurious harmonics are not produced. Peak shifting by small amounts does occur due to overlap between neighbouring peaks or due to overlap between a peak and the sidebands of a neighbouring peak. The accuracy with which the amplitudes A_i in equation (17) are reproduced is also governed by the degree of overlap between neighbouring peaks, when it is substantial there is considerable distortion of the amplitudes.

It has been found that Fourier transformation is an excellent method for analyzing the frequencies ω_i . It does not provide a good method for determining the exponential growth factors λ_i . The question of the amplitudes is complicated by the presence of the exponential terms since the height of a peak in the Fourier transform is controlled by both the amplitude factors A_i and the λ_i . In numerical experiments with all the $\lambda_i=0$ it has been found that amplitudes are reproduced to an accuracy of about 10% in the case of isolated peaks but amplitudes are extremely sensitive to overlap and no physical significance should be attributed to the heights of peaks that are close to other peaks.

The accuracy of the analysis can be improved by taking a larger number of oscillations, the width of the peaks is reduced, but a limit is set by the amount of time it takes a computer to do the calculation. An excellent way to reduce overlap between different peaks and their respective sidebands is to suppress the sidebands. One way of doing this is to impose a 'cosine window' on to the data.

Another problem is the question of noise in the data. If it is a random fluctuation superimposed on to the de Haas-van Alphen oscillations, it is not too serious provided its amplitude is not too large. Fourier transformation is an excellent way of smoothing out this type of noise. Also the method of least squares curve fitting adopted in the program that has been developed eliminates a great deal of this noise.

A far more serious type of noise is that arising from the uncertainty involved in the instrumental measurement of the magnetic field strength H . In a typical experiment the magnetic field is increasing steadily with time and its strength is measured at regular intervals of time. The true values of the field are in a perfect monotonic sequence. If the instrumental errors are such that the recorded values of the magnetic field are not in a monotonic sequence, then the numbers generated by the program are meaningless. If order reversal occurs for about one point in ten it probably does

not matter too much, but if it happens more often it can ruin the data so far as the program is concerned. It is essential to take steps to prevent this noise from being too severe. It is possible to introduce an operation into the program which smooths out this noise, but there are limits as to how far this can be taken.

Mathematical properties of the Fourier transform

An arbitrary function of x , that satisfies certain conditions that in practically all cases of physical interest are fulfilled, can be represented by the expression

$$f(x) = \frac{1}{2\pi} \int_{-\infty}^{\infty} F(\omega) e^{j\omega x} d\omega$$

where

$$F(\omega) = \int_{-\infty}^{\infty} f(x) e^{-j\omega x} dx .$$

The function $F(\omega)$ is called the Fourier transform of the function $f(x)$. The relationship can be expressed

$$f(x) \leftrightarrow F(\omega) .$$

$F(\omega)$ is a complex function of ω and can be split up into its real and imaginary parts

$$F(\omega) = R(\omega) + jX(\omega) ,$$

where

$$R(\omega) = \int_{-\infty}^{\infty} f(x) \cos \omega x dx , \quad X(\omega) = - \int_{-\infty}^{\infty} f(x) \sin \omega x dx .$$

$F(\omega)$ can also be written as

$$F(\omega) = A(\omega) \exp(j\phi(\omega)).$$

The function $A(\omega)$ is called the Fourier spectrum of $f(x)$, $A^2(\omega)$ the energy spectrum and $\phi(\omega)$ the phase angle.

$$A(\omega) = [(R(\omega))^2 + (X(\omega))^2]^{\frac{1}{2}}$$

$$\phi(\omega) = \arctan(-X(\omega)/R(\omega)).$$

Some simple properties of the Fourier transform are expressed by the following theorems.

Linearity. If $F_1(\omega)$ and $F_2(\omega)$ are the transforms of the functions $f_1(x)$ and $f_2(x)$ respectively and a_1, a_2 are two arbitrary constants then

$$a_1 f_1(x) + a_2 f_2(x) \leftrightarrow a_1 F_1(\omega) + a_2 F_2(\omega),$$

the extension to finite sums is obvious.

Displacement. If the function $f(x)$ is shifted by a constant x_0 , then its Fourier spectrum remains the same but a linear term $(-x_0\omega)$ is added to its phase angle.

$$f(x-x_0) \leftrightarrow F(\omega) e^{-jx_0\omega} = A(\omega) e^{j[\phi(\omega)-x_0\omega]}$$

Frequency shifting. With ω_0 a real constant the Fourier transform of $e^{j\omega_0 x} f(x)$ is obtained by shifting $F(\omega)$ by ω_0 .

$$e^{j\omega_0 x} f(x) \leftrightarrow F(\omega-\omega_0).$$

This theorem can be used to derive the Fourier transform $A_c(\omega) e^{j\phi_c(\omega)}$ of a modulated signal $f(x) \cos(\omega_0 x)$ in terms of the Fourier integral of its envelope $f(x)$,

$$f(x) \cos \omega_0 x \leftrightarrow \frac{f(\omega - \omega_0) + F(\omega + \omega_0)}{2} = A_c(\omega) e^{j\phi_c(\omega)}, \quad (18)$$

similarly

$$f(x) \sin \omega_0 x \leftrightarrow \frac{F(\omega - \omega_0) - F(\omega + \omega_0)}{2j} = A_s(\omega) e^{j\phi_s(\omega)}. \quad (19)$$

A typical term of equation (17) is of the form $f(x) \sin(\omega_0 x + \alpha)$, where $f(x)$ is an envelope function which is zero outside the limits $x_1 < x < x_2$ and it is assumed that the exponential growth function as well as the finite length of the data is incorporated into $f(x)$.

$$\text{Let } f(x) \sin(\omega_0 x + \alpha) \leftrightarrow \Phi(\omega),$$

where

$$f(x) \leftrightarrow F(\omega) = A(\omega) \exp(j\phi(\omega)).$$

Using equations (18) and (19)

$$\Phi(\omega) = F(\omega - \omega_0) \frac{\exp(j\alpha)}{2j} - F(\omega + \omega_0) \frac{\exp(-j\alpha)}{2j},$$

$$\Phi^*(\omega) = F^*(\omega - \omega_0) \frac{\exp(-j\alpha)}{(-2j)} - F^*(\omega + \omega_0) \frac{\exp(j\alpha)}{(-2j)}.$$

Thus

$$|\Phi(\omega)|^2 = \frac{1}{4} \left\{ |F(\omega - \omega_0)|^2 + |F(\omega + \omega_0)|^2 - F(\omega + \omega_0) F^*(\omega - \omega_0) e^{-2j\alpha} - F^*(\omega + \omega_0) F(\omega - \omega_0) e^{2j\alpha} \right\}.$$

Let $\Phi(\omega)$ have an amplitude function $c(\omega)$ so that

$$\Phi(\omega) = C(\omega) e^{j\psi(\omega)}.$$

Therefore

$$C(\omega)^2 = \frac{1}{4} \left\{ |A(\omega - \omega_0)|^2 + |A(\omega + \omega_0)|^2 - 2R_e(A(\omega - \omega_0)A(\omega + \omega_0) \exp[j(\phi(\omega + \omega_0) - \phi(\omega - \omega_0) - 2\alpha)]) \right\}. \quad (20)$$

If the envelope function is such that its Fourier spectrum $A(\omega)$ has a high narrow peak centred on $\omega=0$, with a peak width narrow compared with ω_0 the modulating frequency, then the Fourier spectrum $C(\omega)$ of the modulated envelope function will have peaks centred almost exactly at $\omega=\omega_0$ and $\omega=-\omega_0$, because

$$|C(\omega_0 + \Delta\omega)|^2 = \frac{1}{4} \{ |A(\Delta\omega)|^2 + |A(2\omega_0 + \Delta\omega)|^2 - 2A(\Delta\omega) A(2\omega_0 + \Delta\omega) \cos(\phi(2\omega_0 + \Delta\omega) - \phi(\Delta\omega) - 2\alpha) \}. \quad (21)$$

If $A(2\omega_0)$ is negligibly small compared with $A(0)$, then $C(\omega_0 + \Delta\omega)$ will have a maximum almost exactly at $\Delta\omega=0$, that is at $\omega=\omega_0$. The negative frequency has no significance, the Fourier spectrum of any real function is symmetrical about $\omega=0$. The conclusion follows that provided the envelope function has a Fourier spectrum $A(\omega)$ which is a high narrow peak centred on $\omega=0$, then the modulated function has a Fourier spectrum $C(\omega)$ which is effectively $A(\omega)$ but with its peak centred on $\omega=\omega_0$. The width and shape of $C(\omega)$ are almost exactly the same as for $A(\omega)$.

The previous statements do not apply if $A(2\omega_0)$ is not small compared with $A(0)$, in which case the peak of the Fourier spectrum will not be centred at ω_0 . The Fourier spectra of the envelope functions that are to be expected in this particular application of Fourier analysis will always be simple peaks centred at the origin, so if $A(2\omega_0)$ is not

small compared with $A(\omega)$ it means that ω_0 is small compared with the intrinsic width of the peak in $A(\omega)$. This implies that there are very few oscillations in the experimental data in the field range through which the experiment was carried out. If this is the case it is impossible in principle by any method to determine the frequency accurately.

If the experimental conditions are such that the uncertainty in determining a fraction of an oscillation is equal to one oscillation, then to determine a frequency to an accuracy of 1 part in n at least n oscillations are required. This is true in general irrespective of whatever method of measurement is adopted. This theorem is reflected in the Fourier transform method, if there are n oscillations of frequency ω_0 in a particular experimental record, then half the 'peak width' $\approx \frac{\omega_0}{n}$. This can be written $\Delta\omega \approx \frac{\omega_0}{n}$. $\Delta\omega_0$ is practically the same for all the component frequencies in the data and is governed mainly by the length of the experimental record, being inversely proportional to the length of the record. The minimum frequency difference for two frequencies to be unambiguously resolved is when the difference of frequencies is approximately equal to $\Delta\omega_0$. Let there be n_1 oscillations of frequency ω_1 in the record and n_2 of frequency ω_2 . If these frequencies are at the limit of clear resolution by the Fourier transform method,

$$\omega_1 - \omega_2 \approx \Delta\omega_0$$

but $n_1 = \frac{\omega_1}{\Delta\omega_0}$ and $n_2 = \frac{\omega_2}{(\Delta\omega_0)}$, consequently $n_1 - n_2 \approx 1$.

This implies that the limit of clear resolution coincides with the condition of there being just one beat between the two frequencies in the range of the experiment concerned. The point to be emphasized is that the limits of precision of the Fourier transform method are as good as any other conceivable method. If the Fourier transform is unable to clearly resolve two frequencies in the data, no other method will be any more successful.

Non Linearity of the Fourier spectrum

Fourier transformation is a linear operation, but when the amplitude function is calculated this linearity is destroyed. If there is a set of functions of x :

$f_1(x), f_2(x), \dots, f_n(x)$, whose Fourier transforms are $F_1(\omega), F_2(\omega), \dots, F_n(\omega)$, respectively, then the Fourier transform of the sum of these functions is the sum of the Fourier transforms of the functions. Let

$$f_1(x) + f_2(x) + \dots + f_n(x) \leftrightarrow A(\omega)e^{i\phi(\omega)}$$

Using the notation $F_j(\omega) = A_j(\omega)e^{i\phi_j(\omega)}$ it follows that

$$A(\omega)e^{i\phi(\omega)} = \sum_j A_j(\omega)e^{i\phi_j(\omega)}$$

and

$$A(\omega)e^{-i\phi(\omega)} = \sum_i A_i(\omega)e^{-i\phi_i(\omega)}$$

therefore

$$A(\omega)^2 = \sum_j [A_j(\omega)]^2 + 2 \sum_{\substack{j,k \\ j < k}} A_j(\omega) A_k(\omega) \cos(\phi_j(\omega) - \phi_k(\omega))$$

so that the amplitude functions do not combine⁽²²⁾ linearly.

If in the Fourier transform each of the $A_i(\omega)$ is a narrow peak centred on ω_i and all the peaks are well isolated so that mixing terms between the various peaks are very small, then to a very good approximation $A(\omega_i) = A_i(\omega_i)$. However there may be so many peaks that the mixing between them is substantial, in this case spurious peaks could occur although they are usually easy to detect because their characteristic line width is usually wrong. In any case if two peaks occur close together there is interference between them, not just simple superposition.

If there are two frequencies in the data that individually possess Fourier transforms $A_1(\omega)e^{i\phi_1(\omega)}$ and $A_2(\omega)e^{i\phi_2(\omega)}$, then following equation (22),

$$A^2(\omega) = A_1^2(\omega) + A_2^2(\omega) + 2A_1(\omega)A_2(\omega)\cos(\phi_1(\omega) - \phi_2(\omega))$$

so

$$|A_1(\omega) - A_2(\omega)| \leq A(\omega) \leq |A_1(\omega) + A_2(\omega)|$$

Obviously if the frequencies are to be resolved accurately $A_1(\omega)$ and $A_2(\omega)$ must not be large simultaneously. It has been found in numerical experiments that when peaks are at a separation which is of the same order of magnitude as their intrinsic line width, they are subject to shifting and

distortion. This sets a limit to the resolving power of the method.

Characteristics of the amplitude peaks

The characteristics of the amplitude peaks are largely determined by the nature of the envelope functions. Ideally the Fourier spectrum of an envelope function should possess a high narrow peak centred on $\omega=0$. The simplest function to consider is a rectangular window, it is also a good approximation to the shape of the envelope functions that are often obtained in practise.

The rectangular window

This function can be defined by $f(x)=1$ in the range $x_1 < x < x_2$; $f(x) = 0$ outside this range. Let $x_2 - x_1 = b$. Then

$$F(\omega) = \int_{x_1}^{x_2} e^{-j\omega x} dx = \frac{2}{\omega} e^{-j\omega x_1} e^{-j\omega \frac{b}{2}} \sin\left(\frac{\omega b}{2}\right),$$

$$|F(\omega)|^2 = b^2 \frac{\sin^2\left(\frac{\omega b}{2}\right)}{\left(\frac{\omega b}{2}\right)^2}$$

so that

$$A(\omega) = b \frac{|\sin\left(\frac{\omega b}{2}\right)|}{\left(\frac{\omega b}{2}\right)} .$$

$A(\omega)$ which is in fact the characteristic amplitude function for single slit diffraction is illustrated in Figure (II,1). There is a central peak of height b centred at $\omega=0$. This

peak is of intrinsic width $\Delta\omega = \frac{4\pi}{b}$. The successive sidebands whose amplitudes decrease approximately as $(\frac{b}{\pi})\frac{1}{n}$ are spaced out at intervals of $\delta\omega = \frac{2\pi}{b}$. It is possible to distinguish true peaks from sidebands in this case because they are twice as wide. The presence of sidebands is usually a nuisance. The amplitude of the first sideband is approximately 30% of the amplitude of the main peak. However sometimes their presence can be of advantage when there is much noise in the data. Free peaks are surrounded by a characteristic array of sidebands which identifies them. If the de Haas-van Alphen data is of the form $f(x)\sin(\omega_0 x)$, where $f(x)$ is a rectangular window function and ω_0 is a modulating frequency, the peak will be shifted to $\omega = \omega_0$ and the sidebands will be displaced with it.

If there are n oscillations in the experimental data corresponding to the frequency ω_0 , then $\omega_0 = (\frac{2\pi}{b})n$, but the width of a sideband is $(\frac{2\pi}{b})$ and one half the width of the central peak is also $(\frac{2\pi}{b})$. The general result follows that if there are n oscillations in the experimental data corresponding to a component frequency ω_0 , there will be $(n-1)$ sidebands between the central peak and the origin. The resolving power can be identified by:

Resolving power = (Frequency of main peak) / ($\frac{1}{2}$ width of peak).

It follows that resolving power equals n .

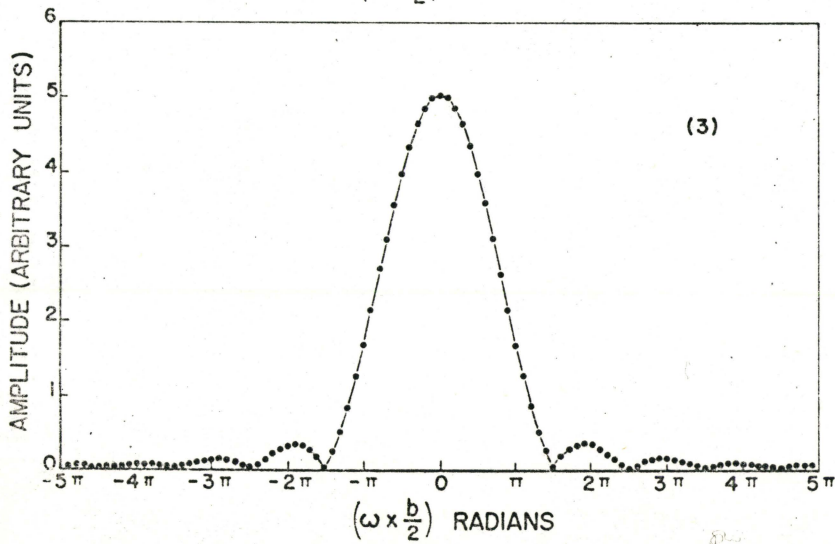
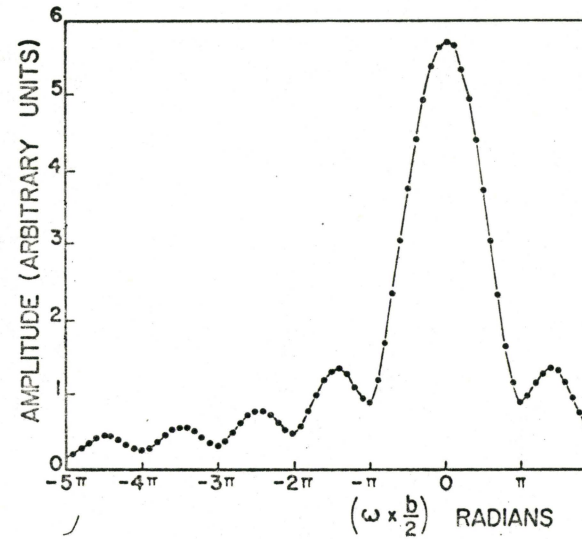
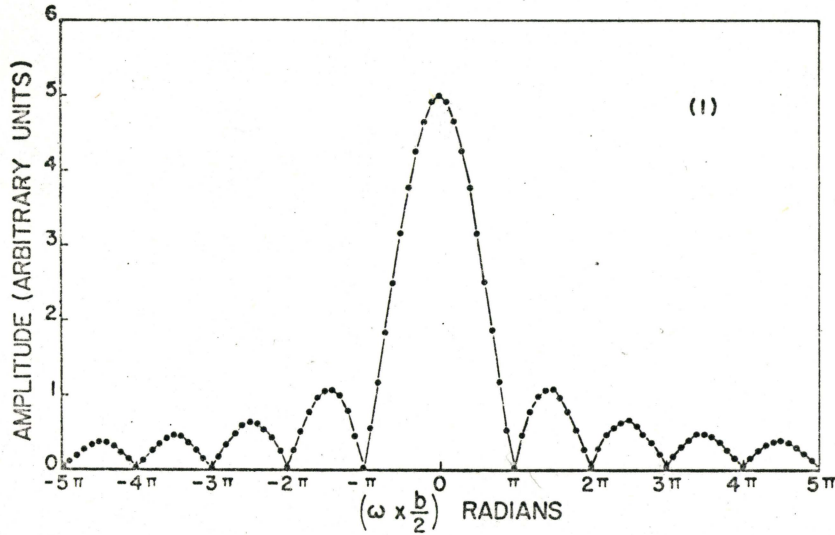


Fig. (II.1) Rectangular window

Fig. (II.2) Exponential window

Fig. (II.3) Cosine window function

The truncated exponential envelope function

A more general type of envelope function is of the form $y = e^{-\lambda x}$ truncated between $x=x_1$ and $x=x_2$. In this case

$$F(\omega) = \int_{x_1}^{x_2} e^{-\lambda x} e^{-j\omega x} dx ,$$

$$F(\omega) = - \frac{1}{(\lambda + j\omega)} e^{-(\lambda + j\omega)x_1} (e^{-(\lambda + j\omega)b} - 1) .$$

where $b = (x_2 - x_1)$.

$$|F(\omega)|^2 = \frac{1}{(\lambda^2 + \omega^2)} e^{-2\lambda x_1} (e^{-2\lambda b} - 2e^{-\lambda b} \cos \omega b + 1)$$

$$|F(\omega)|^2 = 2 \frac{e^{-2\lambda x_1}}{(\lambda^2 + \omega^2)} e^{-\lambda b} (\cosh \lambda b - \cos \omega b) ,$$

$$|F(\omega)|^2 = \frac{4}{(\lambda^2 + \omega^2)} e^{-2\lambda x_1} e^{-\lambda b} \left(\sinh^2 \frac{\lambda b}{2} + \sin^2 \frac{\omega b}{2} \right)$$

Ignoring the constant terms $A^2(\omega)$ varies as

$$P(\omega) = \frac{(\sinh^2 \frac{\lambda b}{2} + \sin^2 \frac{\omega b}{2})}{(\lambda^2 + \omega^2)} .$$

$P(\omega)$ is a function that oscillates between two bounding functions $\phi_1(\omega)$ and $\phi_2(\omega)$ where

$$\phi_1(\omega) = \frac{\sinh^2 \frac{\lambda b}{2}}{(\lambda^2 + \omega^2)}$$

and

$$\phi_2(\omega) = \frac{\sinh^2 \frac{\lambda b}{2} + 1}{(\lambda^2 + \omega^2)}$$

Refer to Figure (II,2) for illustration. $P(\omega)$ oscillates between the bounding functions with frequency $\Delta\omega = \frac{2\pi}{b}$.

In this case $P(\omega)$ has no zeros, hence $A(\omega)$ has no zeros, unlike the case of the rectangular window function which corresponds to $\lambda = 0$. At $\omega = 0$, $P(\omega)$ is on the lower bounding function and at $\omega = \pm \frac{\pi}{b}$ it is in tangential contact with the upper bounding function and it is necessary to prove that the highest point of $P(\omega)$ is at the origin.

$P(\omega)$ varies as

$$\frac{(\sinh^2 \frac{\lambda b}{2} + \sin^2 \frac{\omega b}{2})}{((\frac{\lambda b}{2})^2 + (\frac{\omega b}{2})^2)} = \frac{f_1(\omega)}{f_2(\omega)}$$

Now $f_1(0) > f_2(0)$, but $f_1'(\omega) = \frac{b}{2} \sin \omega b$ and $f_2'(\omega) = \frac{b}{2}(\omega b)$. Therefore $f_1'(\omega) \leq f_2'(\omega)$ in the interval $0 \leq \omega \leq \frac{\pi}{b}$, so that $P(\omega)$ decreases steadily in this interval.

To summarize, the truncated exponential function has the peak of its Fourier spectrum $A(\omega)$ at the origin as required, there are no zeros in $A(\omega)$, the 'effective linewidth' is dominated by the bounding functions $\frac{1}{(\lambda^2 + \omega^2)}$ when λ is large and is independent of b . As the uncertainty principle indicates, for large λ the 'effective linewidth' is greater than the value $\frac{2\pi}{b}$ which is obtained when $\lambda=0$. The sidebands which are prominent in the case of the rectangular window function also occur in the more general case manifesting themselves as the oscillations between the two bounding functions.

Suppression of sidebands

If the data $y_i(x_i)$ is multiplied by a cosine function such that

$$y_i \rightarrow Y_i \cos\left(\pi \frac{(x-\bar{x})}{(x_2-x_1)}\right),$$

where x_1 and x_2 are the limits of truncation and $\bar{x} = \frac{(x_1+x_2)}{2}$, then provided the exponential growth factors are not very strong the envelope function is approximately a cosine window. The cosine window differs from the rectangular window in that the width of the central main peak is increased by 50% but the amplitudes of successive sidebands decrease approximately as $\frac{1}{n^2}$ rather than as $\frac{1}{n}$ in the case of the rectangular window.

The cosine window envelope function

If the envelope function is defined by

$$F(x) = \cos\left\{\pi\left(x - \frac{x_1+x_2}{2}\right)/b\right\} \text{ where } b = x_2-x_1,$$

then

$$F(\omega) = \int_{x_1}^{x_2} \cos \frac{\pi}{b} \left(x - \frac{x_1+x_2}{2}\right) e^{-j\omega x} dx.$$

It follows quite readily that

$$|F(\omega)|^2 = \frac{4 \frac{\pi^2}{b^2} \cos^2 \frac{\omega b}{2}}{\left(\frac{2\pi}{b} - \omega^2\right)^2}$$

so that

$$A(\omega) = \frac{\left(\frac{2\pi}{b}\right) \left|\cos \frac{\omega b}{2}\right|}{\left(\frac{\pi^2}{b^2} - \omega^2\right)}$$

The zeros of $A(\omega)$ occur when $\omega = \frac{\pi}{b} + n(\frac{2\pi}{b})$. However the zero at $\omega = \frac{\pi}{b}$ is absorbed into the main peak centred at $\omega=0$, because when $\omega = \frac{\pi}{b}$ numerator and denominator are simultaneously zero. Figure (II,3) illustrates $A(\omega)$ in this case.

The 'Gaussian Window' envelope function.

An envelope function which ideally would have no sidebands at all would be a function of the form

$$f(x) = \exp \left\{ -\alpha \left(x - \frac{(x_1 + x_2)}{2} \right)^2 \right\},$$

where α is sufficiently large so that

$$\exp \left\{ -\alpha \frac{(x_2 - x_1)^2}{4} \right\} \ll 1$$

This follows from the relation

$$e^{-\alpha x^2} \leftrightarrow \sqrt{\frac{\pi}{\alpha}} e^{-\omega^2/4\alpha}.$$

However in practise when α is so large that the above condition holds, the amplitude peaks are inconveniently broad. If α is chosen so that $\exp\{-\frac{\alpha}{4}(x_2 - x_1)^2\} \approx \frac{1}{6}$ a significant reduction of sidebands is achieved with a reasonable line-width.

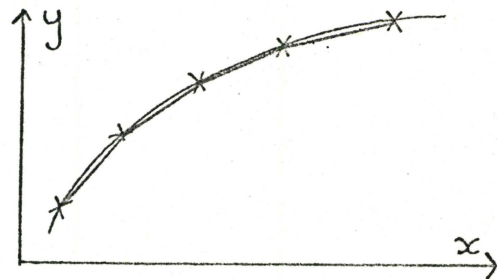
However no final conclusions can be drawn as to the best window function to impose on the data. The cosine window function is probably sufficient in most cases, in any case total suppression of sidebands is not always desirable because they can assist in the identification of the main peaks.

CHAPTER III

DEVELOPMENT OF THE DIGITAL PROGRAM

In the development of any digital program it is important to ensure that the time taken to carry out the required computations should not be so excessive as to be uneconomical. This is especially true of programs intended to compute Fourier transforms where numerous sines and cosines have to be calculated.

Typical data consists of a set of points (X_i, Y_i) distributed along a curve $y = f(x)$. A simple way to compute the Fourier transform of the data is for the program to join successive points by straight line segments so that the smooth curve $y=f(x)$ is approximated by a series of trapezoidal sections. It is very simple to calculate a formula for the Fourier transform of a series of trapezoidal sections and a program based on this principle could certainly be developed, but it would take too much time to carry out the computations when the number of data points is large. One of the most time consuming operations the computer has to perform



is to calculate sines and cosines. If the number of data points is N_1 and the number of frequencies is N_2 then the number of sines and cosines that need to be calculated is equal to $N_1 \times N_2$. It is essential to devise a method whereby the effective number of data points is reduced before the Fourier transform is calculated.

Another disadvantage of the trapezoidal method is that unless the data points are very close together the series of straight line segments is not a very good approximation to the smooth curve $y = f(x)$. It is also a disadvantage that the trapezoidal method does not have the capacity to smooth out noise at an early stage in the computation.

Point reduction by polynomial arcs

If it is possible to approximate the data by a series of polynomial arcs, the effective number of data points can be much reduced. For example, if there are on average eight points along each arc, then the effective number of data points is reduced by a factor of eight because it is only necessary to calculate the sine and cosine at the end points of each arc. In the program that has been developed the data is replaced by a series of parabolic arcs that are calculated by a least squares procedure. In principle the method could be extended to compute polynomial arcs of any order, clearly a cubic

polynomial arc can approximate a longer stretch of data than a parabolic arc and thus effect a more efficient point reduction. However, it takes more time to calculate higher order polynomials, for this reason the present program is restricted to calculating parabolic arcs.

Clearly a parabolic arc is a closer approximation to the true curve passing through a set of data points than a series of straight line segments can be. To some extent a parabolic arc that is computed by a least squares procedure will tend to ignore the noise fluctuations thus smoothing the data to some extent.

Procedure for calculating the polynomial arcs

An efficient way to calculate the n^{th} order polynomial that gives the best least squares fit to a series of data points is to make use of a system of orthogonal Chebyshev polynomials. Suppose there is a series of N consecutive data points

$$(x_1, y_1), (x_2, y_2), \dots, (x_N, y_N) .$$

Let the sequence of polynomials

$$\phi_0(x), \phi_1(x), \dots, \phi_n(x) ,$$

where $\phi_k(x)$ is of order k , be an orthogonal system of functions with respect to the system of points x_1, x_2, \dots, x_N .

This means that

$$\sum_{i=1}^N \phi_{\mu}(x_i) \phi_{\nu}(x_i) = [\phi_{\mu}(x) \phi_{\nu}(x)] = 0$$

for $\mu \neq \nu$.

Any n^{th} order polynomial can be uniquely specified by the expression

$$\phi(x) = C_0 \phi_0(x) + C_1 \phi_1(x) + \dots + C_n \phi_n(x) .$$

The deviation Δ of this polynomial from the actual data points can be expressed by

$$\Delta = \sum_{i=1}^N (y_i - \phi(x_i))^2 ,$$

$$\Delta = \sum_{i=1}^N (y_i - C_0 \phi_0(x_i) - C_1 \phi_1(x_i) - \dots - C_n \phi_n(x_i))^2, \quad (23)$$

$$\begin{aligned} \frac{\partial \Delta}{\partial C_j} &= \sum_{i=1}^N 2(y_i - C_0 \phi_0(x_i) - C_1 \phi_1(x_i) - \dots - C_n \phi_n(x_i)) \\ &\quad \times (-\phi_j(x_i)) . \end{aligned}$$

Because of the condition of orthogonality this reduces to

$$\frac{\partial \Delta}{\partial C_j} = 2 \sum_{i=1}^N \{-y_i \phi_j(x_i) + C_j (\phi_j(x_i))^2\}.$$

But if Δ is at a minimum $\frac{\partial \Delta}{\partial C_j} = 0$, $j = 0, 1, 2, \dots, n$ therefore

$$C_j = \frac{\sum_{i=1}^N y_i \phi_j(x_i)}{\sum_{i=1}^N [\phi_j(x_i)]^2}, \quad j = 0, 1, 2, \dots, n.$$

Thus once the orthogonal polynomials have been generated it is very easy to calculate the coefficients \bar{C}_j appropriate to that polynomial which has the least squares deviation from the actual data points.

$$\bar{c}_j = \frac{\sum_{i=1}^N y_i \phi_j(x_i)}{\sum_{i=1}^N [\phi_j(x_i)]^2} = \frac{[y \phi_j(x)]}{[\phi_j(x) \cdot \phi_j(x)]} \quad (24)$$

The set of polynomials can be generated as follows. We put $\phi_0(x)=1$. We can regard $\phi_1(x)$ as a linear combination of x and $\phi_0(x)$, so that:

$$\phi_1(x) = x + b\phi_0(x),$$

where b is chosen so that

$$[\phi_0(x) \cdot \phi_1(x)] = 0,$$

but this implies

$$\sum_{i=1}^N 1 \cdot (x+b) = 0,$$

thus

$$b = - \frac{\sum_{i=1}^N x}{N} = - \bar{x}.$$

Therefore

$$\phi_1(x) = x - \bar{x} = x - \frac{[x]}{N}.$$

Now put

$$\phi_2(x) = x^2 + b_1 \phi_1(x) + b_0 \phi_0(x),$$

since ϕ_2 is orthogonal to both $\phi_1(x)$ and $\phi_0(x)$ it follows that

$$b_0 = - \frac{[x^2]}{N}, \quad b_1 = - \frac{[x^2 \phi_1(x)]}{[(x-\bar{x})^2]}$$

so

$$\phi_2(x) = x^2 - \frac{[x^2(x-\bar{x})]}{[(x-\bar{x})^2]} (x-\bar{x}) - \frac{[x^2]}{N}.$$

Proceeding in this way it can be shown that

$$\phi_m(x) = x^m - \frac{[x^m \phi_{m-1}(x)]}{[\phi_{m-1}(x) \phi_{m-1}(x)]} \phi_{m-1}(x) - \dots - \frac{[x^m]}{N} .$$

One virtue of this method is that if the best m^{th} order polynomial has been determined and it is desired to calculate the best $(m+1)^{\text{th}}$ order polynomial. It is only necessary to calculate $\phi_{m+1}(x)$ and \tilde{C}_{m+1} . The other functions $\phi_k(x)$, $k = 0, 1, \dots, m$ and the coefficients $\tilde{C}_0, \tilde{C}_1, \dots, \tilde{C}_m$ remain the same. Using equations (23) and (24) the amount by which the closest n^{th} order polynomial to the data points deviates from these points is given by Δ_{\min} , where

$$\begin{aligned} \Delta_{\min} = & \sum_{i=1}^N y_i^2 - \tilde{C}_0^2 [\phi_0(x) \cdot \phi_0(x)] - \tilde{C}_1^2 [\phi_1(x) \cdot \phi_1(x)] \\ & - \dots - \tilde{C}_n^2 [\phi_n(x) \cdot \phi_n(x)]. \end{aligned} \quad (25)$$

We see that Δ_{\min} decreases steadily as the order of the polynomial increases.

Basic form of the program

The main principle behind all forms of the program is that the program takes the first three data points and calculates the best parabola that passes through these three points. The closeness of fit of this parabola to the actual data points is referred to in the program as CLOSE, in fact CLOSE is equal to Δ_{\min} of equation (25).

If CLOSE is less than a certain number called DELTA, the best parabolas for four points, five points and so on are calculated until it is found that CLOSE is bigger than DELTA. The last parabola for which CLOSE was less than or equal to DELTA is selected. If this parabola extends over m data points the first of which has an x coordinate called $X(\text{LMIN})$ and the last one an x coordinate called $X(\text{LMAX})$, then if the equation of this parabola is given by $\psi(x) = Ax^2 + Bx + C$, the integrals

$$\text{CN}(\omega) = \int_{X(\text{LMIN})}^{X(\text{LMAX})} \psi(x) \cos(\omega x) dx$$

and

$$\text{SN}(\omega) = \int_{X(\text{LMIN})}^{X(\text{LMAX})} \psi(x) \sin(\omega x) dx,$$

are calculated for all the different frequency values ω , for which it is desired to calculate the Fourier transform.

These arrays $\text{CN}(\omega)$ and $\text{SN}(\omega)$ are then stored and the program calculates the next parabolic arc which satisfies the criterion of close enough fit. The last point of the first arc has the same x coordinate as the first point of the second arc, but these two end points are not necessarily coincident. The values $\text{CN}(\omega)$ and $\text{SN}(\omega)$ are calculated for this second parabola and the values added to the old values. Proceeding in this manner the program works its way through the data and eventually the integrated values of the arrays $\text{CN}(\omega)$ and $\text{SN}(\omega)$ are found for the entire range of the data

in the experiment. Once the program reaches the last point in the data the quantities $AFT(\omega)$ are calculated for all the different frequency values

$$AFT(\omega) = \{CN(\omega)^2 + SN(\omega)^2\}^{\frac{1}{2}} .$$

These quantities $AFT(\omega)$ are the amplitudes of the Fourier transform of the data for the frequency values ω . In this way the Fourier spectrum of the data is calculated.

It is a fact that there is always one parabola that passes exactly through three points and it may be that on average in a particular experiment each parabolic arc extends over seven data points. If this is expected to happen it can save time if the program always tries to fit a parabola to six points at its first attempt and then goes on to seven points if the six point parabola is a good fit, but goes back to five points if it is not. In this manner the program eventually finds the correct number of points to which it can approximate a parabolic arc of the desired closeness of fit. The later forms of the program always have an in-built capacity to begin with more than three points at a first attempt if it is thought expedient.

Early forms of the program

The two functions $T_1(X,A)$ and $T_2(X,B,C)$ are defined as statement functions at the beginning of the program. Where $T_1(X,A) = X-A$, $T_2(X,B,C) = X^2 - BX - C$. $T_1(X,A)$ and $T_2(X,B,C)$ are the orthogonal Chebyshev polynomials $\phi_1(x)$

and $\phi_2(x)$ respectively. The coefficients A, B, C are calculated separately each time the program is finding the closest parabola to a given set of data points.

If the set of points is called $(X(1), Y(1)), (X(2), Y(2)), \dots (X(N), Y(N))$, the procedure is as follows. A set of quantities P, Q, R are first calculated where

$$P = \sum_{k=1}^N X(k), \quad Q = \sum_{k=1}^N X(k)^2, \quad R = \sum_{k=1}^N X(k)^3.$$

From these numbers the coefficients A, B, C are calculated thus converting the functions $T_1(X, A)$ and $T_2(X, B, C)$ into the Chebyshev polynomials $\phi_1(x)$ and $\phi_2(x)$ for this particular set of points. These coefficients are given by $A = P/N$, $B = (R - A \times Q) / (Q - N \times A^2)$, $C = \frac{Q}{N} - A \times B$. Next the coefficients $\tilde{C}_0, \tilde{C}_1, \tilde{C}_2$ are calculated using equation (24).

To do this intermediate quantities $P1SUM$ and $P2SUM$ are calculated, where $P1SUM = \sum_{k=1}^N T_1(X(k), A)^2$, $P2SUM = \sum_{k=1}^N T_2(X(k), B, C)^2$. $\tilde{C}_0, \tilde{C}_1, \tilde{C}_2$ are then given by

$$\tilde{C}_0 = \frac{\sum_{k=1}^N Y(k)}{N}, \quad \tilde{C}_1 = \frac{\sum_{k=1}^N Y(k) \times T_1(X(k), A)}{P1SUM},$$

$$\tilde{C}_2 = \frac{\sum_{k=1}^N Y(k) \times T_2(X(k), B, C)}{P2SUM}$$

The parabola has now been calculated, its closeness of fit is given by equation (25)

$$\text{CLOSE} = \sum_{k=1}^N Y(k)^2 - \tilde{C}_0^2 \times N - \tilde{C}_1^2 \times \text{P1SUM} - \tilde{C}_2^2 \times \text{P2SUM}. \quad (26)$$

If this is a parabola for which the program is going to calculate the $\text{CN}(\omega)$ and the $\text{SN}(\omega)$ arrays, it is first converted to the form $A^1 X^2 + B^1 X + C^1$, where $A^1 = \tilde{C}_2$, $B^1 = \tilde{C}_1 - \tilde{C}_2 \times B$, $C^1 = \tilde{C}_0 - \tilde{C}_1 \times A - \tilde{C}_2 \times C$, and then the necessary computations to calculate the $\text{CN}(\omega)$ and $\text{SN}(\omega)$ for this particular parabolic arc are carried out.

It was found that the program worked very well in this form when it was used to calculate the Fourier transform of synthetic data, but some small modifications were found to be required when it was used for real data.

Some later modifications of the program

When the program was used to analyze some real de Haas-van Alphen data it was found that it was not calculating the parabolas properly. The average number of data points on each parabolic arc should be controlled by the closeness of fit parameter DELTA. When DELTA is small the number of points should be less than when DELTA is large. The quantity CLOSE is always greater than or equal to zero if the calculations are carried out without errors. It was discovered that the number of points on each parabolic arc was always larger than expected and seemed to be very insensitive to the value of DELTA. CLOSE was also found to be frequently negative. The reason for these errors was that there were too many significant figures in the magnetic

field variables. In a typical experiment there may be a thousand field measurements taken in a range from 50,000 gauss to 55000 gauss. This means that the magnetic field H needs 5 significant figures to describe it adequately. But in the program $X = \frac{1}{H}$, therefore the X values also have to be specified to 5 significant figures. Now the quantity B is calculated using the formula

$$B = (R - A \times Q) / (Q - N A^2),$$

R and $(A \times Q)$ are very nearly equal to one another and if the field variables need five significant figures to differentiate them from each other it can happen that R and $(A \times Q)$ differ only in the tenth significant figure or worse. But the computer can only work to an accuracy of eight or nine significant figures so it follows that very serious errors in the calculation may result. The denominator $(Q - N \times A^2)$ could also be in error for the same reason. Once B is calculated incorrectly practically all subsequent quantities calculated will be erroneous.

This problem was overcome in the following way. If there is a set of points with X coordinates $X(1), X(2), \dots, X(N)$ to which the program is attempting to fit a parabolic arc, it is possible to reduce the number of significant figures by moving the origin of X temporarily to $X(1)$, so that the new X coordinates will be $0, X(2) - X(1), \dots, X(N) - X(1)$.

The program will now calculate the parabola

$$Y = A^1(X-X(1))^2 + B^1(X-X(1)) + C^1.$$

It is then a simple matter to shift the origin back again and express the parabola in the correct form

$$Y = A'' X^2 + B'' X + C'' .$$

When this modification was built into the program it usually worked properly even when there were many field values measured over a small range of field.

To ensure that CLOSE could not be negative, it was not calculated using equation (26) but was instead calculated in an equivalent positive definite form

$$CLOSE = \sum_{k=1}^N (Y(k) - [A'' X(k)^2 + B'' X(k) + C''])^2.$$

CHAPTER IV

TESTING PROGRAM USING ARTIFICIAL DATA

The program was tested by making it generate artificial data of known analytic form and then calculating the Fourier transform of this data. In a particular example it was made to generate the function.

$$\begin{aligned} F(x) = & 3 \sin(200x + 0.21) + 3.2 \sin(390x + 0.45) \\ & + 3.1 \sin(400x + 0.77) + 0.2 \sin(460x + 0.61) \\ & + 1.9 \sin(540x + 0.70) + 2.4 \sin(610x - 0.35) \\ & + 2.8 \sin(615x + 0.38) + 3 \sin(740x + 0.09) \\ & + 3.2 \sin(820x + 0.32) . \end{aligned}$$

The values of x ranged from 0.003 to 0.600 increasing in steps of 0.001.

Figure (IV,1) is a graph of this function, Figures (IV,2), (IV,3) and (IV,4) show the Fourier spectrum $A(\omega)$ plotted as a function of ω for various frequency ranges.

The upper graph in each case refers to a rectangular window function, the middle graph to a cosine window function and the lower graph to a strong Gaussian window function where $F(x)$ has been multiplied by $\text{EXP}(-(x-\bar{x})^2/0.04)$, \bar{x} is the mid-point of the range of x . These graphs illustrate the very great reduction in the amplitudes of the sidebands

achieved by using a cosine or a Gaussian window function.

It is seen that in all cases the component frequencies have been analysed with the exception of the frequency at $\omega = 460$ which does not show up with a rectangular window because it has a very low amplitude and the sidebands from neighbouring peaks are too large. However this frequency shows up when the cosine and Gaussian window functions are used. The peaks at $\omega = 390$ and $\omega = 400$ have been resolved but they are so close to one another that peak displacement has occurred together with amplitude distortion. The two frequencies at $\omega = 600$ and $\omega = 615$ have not been resolved and have merged into a single peak about twice as broad as an ordinary peak.

The relative amplitudes A of the various peaks together with their frequencies ω are tabulated in Table (IV,1), the columns in the Table refer to the absolute values of A and ω as they occur in $F(x)$ and to the values of A and ω obtained using the different window functions. In each case the amplitude of the peak near $\omega = 200$ has been taken to be unity.

With all three window functions the peaks at $\omega = 390$ and $\omega = 400$ have been displaced to $\omega = 387$ and $\omega = 403$ respectively, this is a typical case of peak displacement. The errors in the relative amplitudes are seen to be large for peaks with close neighbours. However

the relative amplitudes for well isolated peaks are always close to the true values deviating from them by two or three percent.

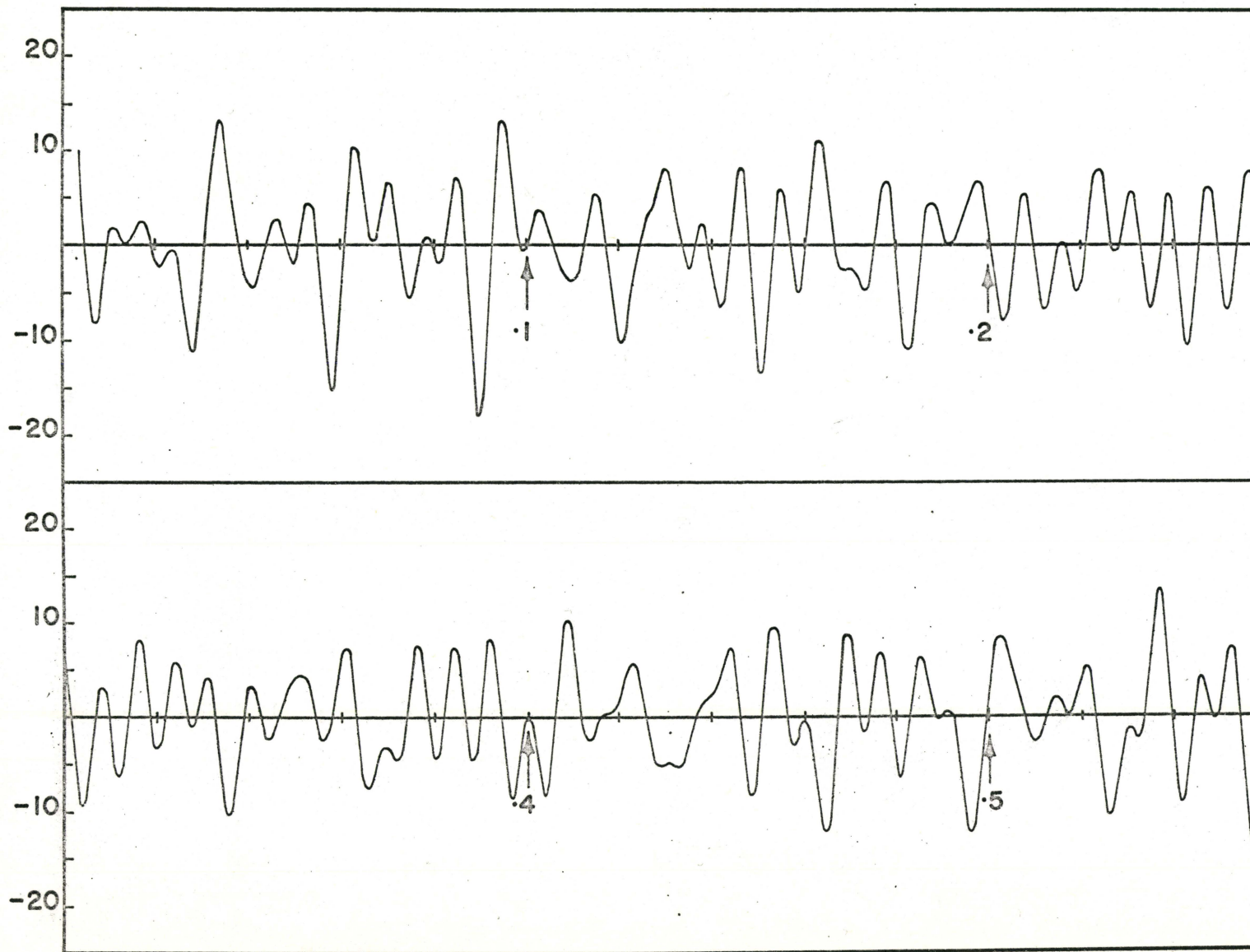


Fig. (IV.1)

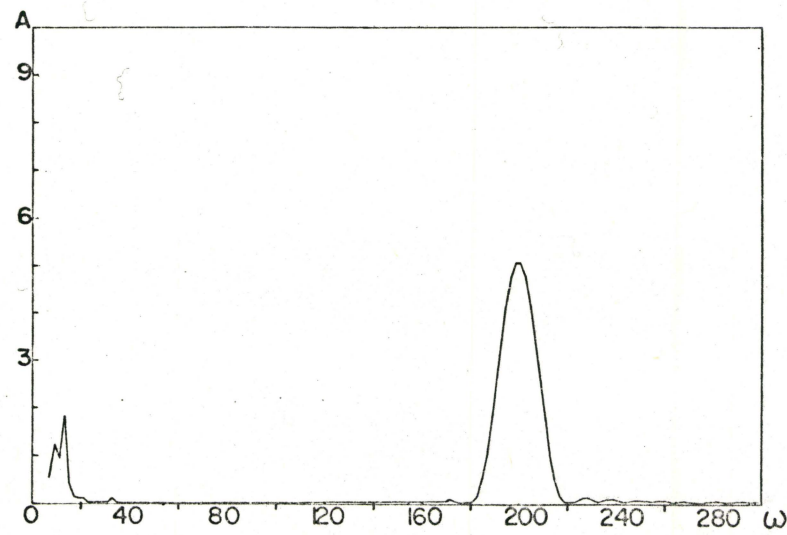
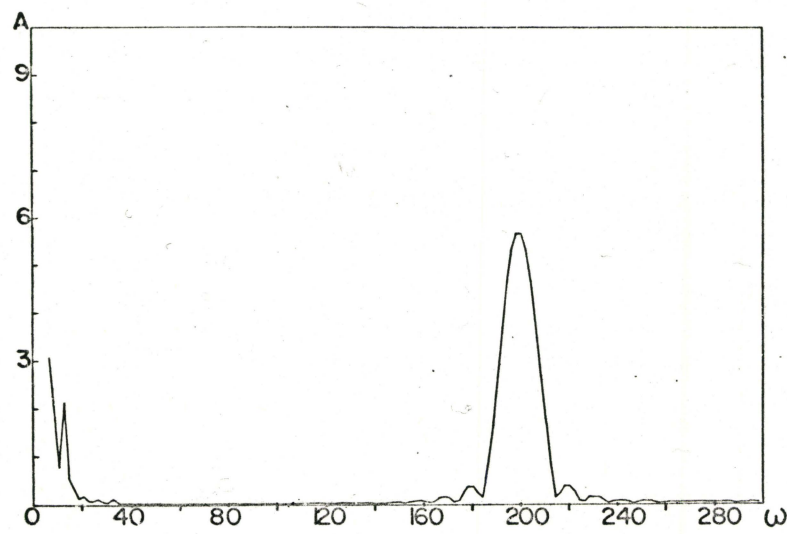
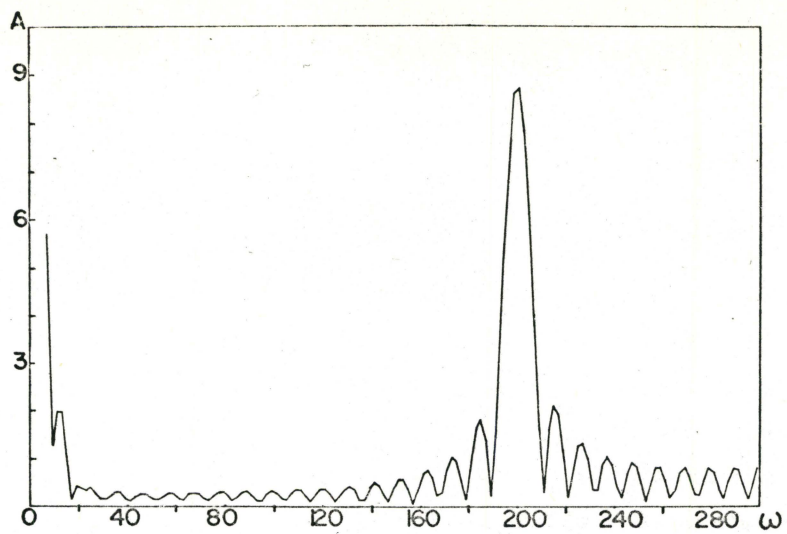


Fig. (IV.2)

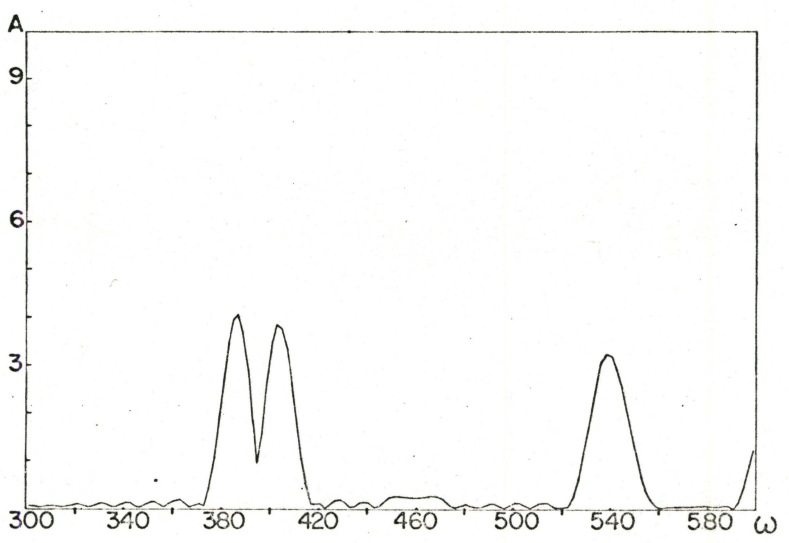
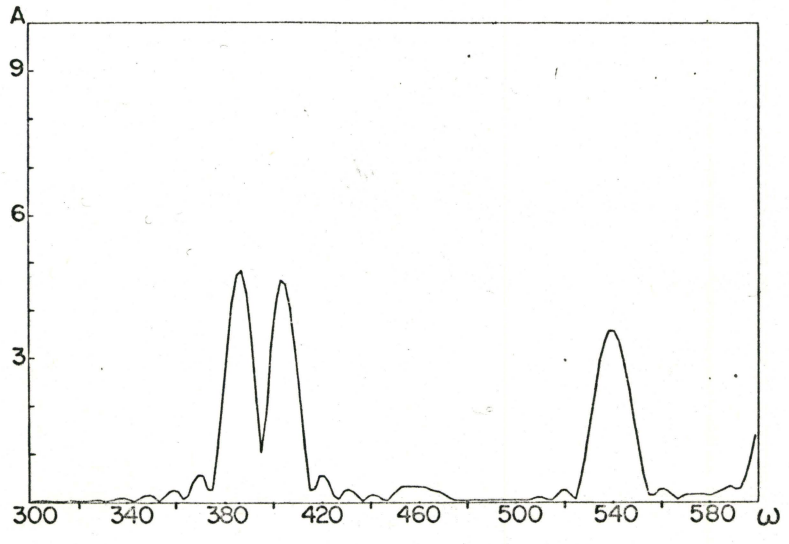
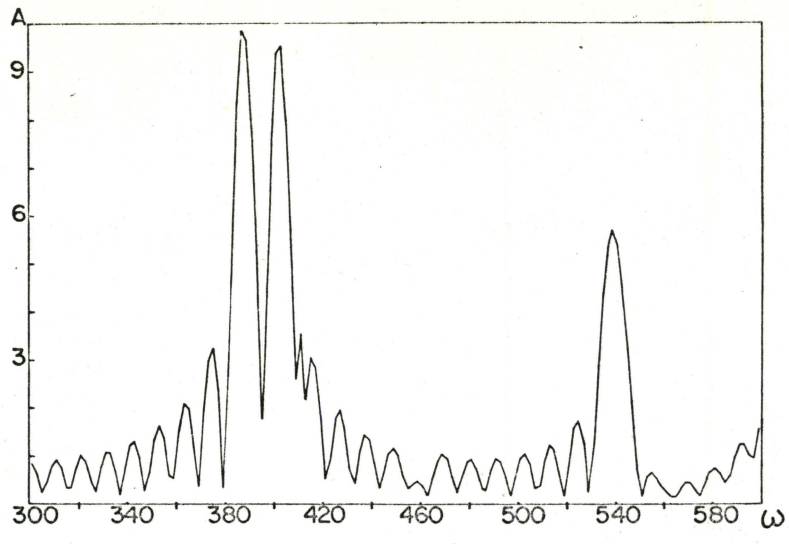


Fig. (IV.3)

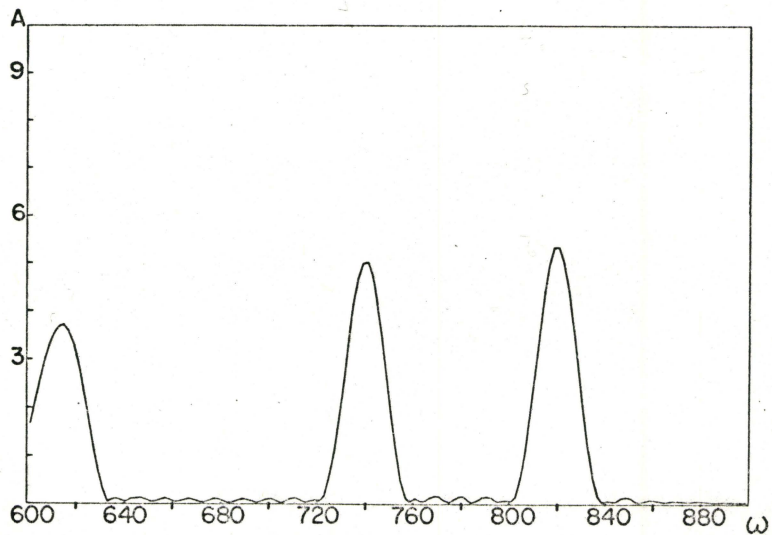
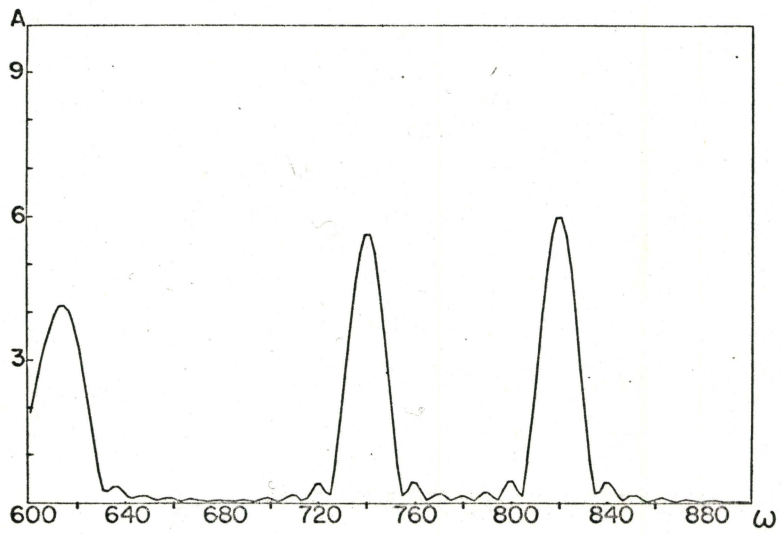
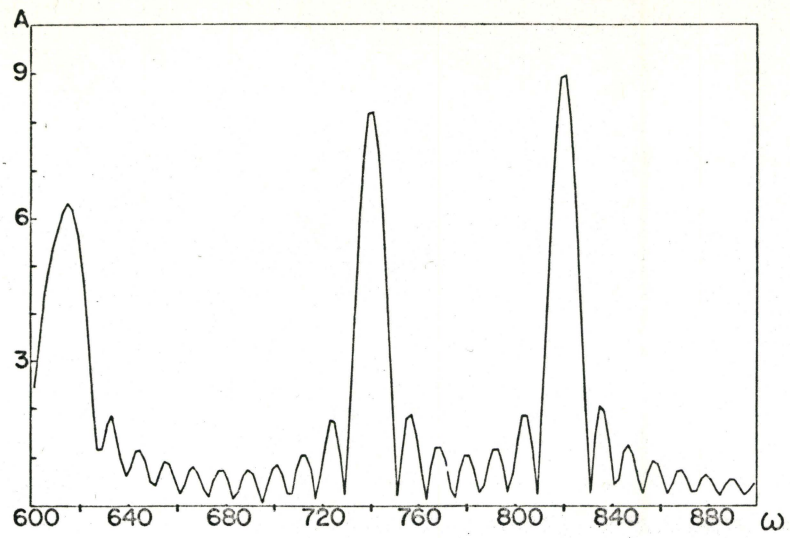


Fig. (IV.4)

TABLE (IV, 1)

Tabulated values of frequencies ω and relative amplitudes A of the Fourier transform.

Absolute values		Rectangular window		Cosine window		Gaussian window	
ω	A	ω	A	ω	A	ω	A
200	1.000	200	1.000	200	1.000	200	1.000
390	1.066	387	1.125	387	0.850	387	0.802
400	1.033	403	1.091	403	0.815	403	0.752
460	0.066	[Unresolved]		457	0.058	460	0.049
540	0.633	539	0.655	540	0.629	540	0.634
610	0.800	[merges with peak at $\omega = 615$]					
615	0.933	615	0.725	615	0.729	615	0.732
740	1.000	740	0.942	740	0.994	740	0.990
820	1.066	820	1.022	820	1.061	820	1.049

CHAPTER V

APPLICATION OF THE PROGRAM TO REAL DATA

The program has been used to analyse data obtained using a mercury crystal. The Fermi surface of mercury has been discussed by Dixon¹⁰; some of the nomenclature of the latter will be used.

Figures (V,1), (V,2), (V,3) all relate to experimental orientations with the magnetic field within a few degrees of the trigonal-bisectrix plane. In each case the upper graph is a photograph of the experimental data with the lower graph a photograph of the computer output.

Figure (V,1) shows some well defined β oscillations, by a simple hand analysis it can be seen that the number of oscillations in the field range between 1.322 Tesla and 3.250 Tesla is almost exactly 34 corresponding to a dominant frequency of 477 (radians)TESLA. The Fourier analysis agrees very well with the simple hand analysis, revealing this strong dominant frequency together with the first and second harmonic. There are no other significant components in this particular experimental trace.

Figure (V,2) shows some well defined τ oscillations together with a very low frequency superimposed upon them, the low frequency is probably a β oscillation. In this case there

are 63τ oscillations in the field range from 4.470 Tesla to 5.185 Tesla corresponding to a frequency of 12800 (radians)TESLA agreeing with the Fourier analysis.

There are approximately 3β oscillations in this field range corresponding to a frequency of 600 (radians)TESLA, the group of peaks appearing in the Fourier analysis in the frequency range below 100 (radians)TESLA is partly due to the β oscillations, however the Fourier analysis is always unreliable at extremely low frequencies.

It is obvious that there must be some higher frequency components in the original data but to resolve them by simple hand analysis would be impossible. The Fourier transform shows a group of frequencies near 22500 (radians)TESLA, these are probably due to α orbits. The reason for there being a group of these peaks is probably that the orientation is not exactly in a symmetry plane and two pieces of the Fermi surface are not exactly degenerate.

Figure (V,3) is an example of an extremely bad experimental run where there was a great deal of noise in the signal, there seems to be a highly distorted dominant frequency in the record with approximately 37 oscillations in the field range from 5.060 Tesla up to 5.360 Tesla corresponding to a frequency of 20,800 (radians)TESLA. A sharp peak very close to this frequency shows up clearly in the Fourier analysis, this

peak is probably due to an α orbit. The higher frequency peaks are unidentified, the one near 41,000 (radians)TESLA is probably a first harmonic.

It sometimes happens that when real data is being analysed the oscillations that are to be studied are superimposed upon a much larger slowly varying background. When this happens the background can be effectively removed by making the program calculate the best parabolic fit to the entire set of data points and then subtracting off this parabola. It is sometimes necessary to have the data treated in this way before being processed by the main Fourier analysis program.

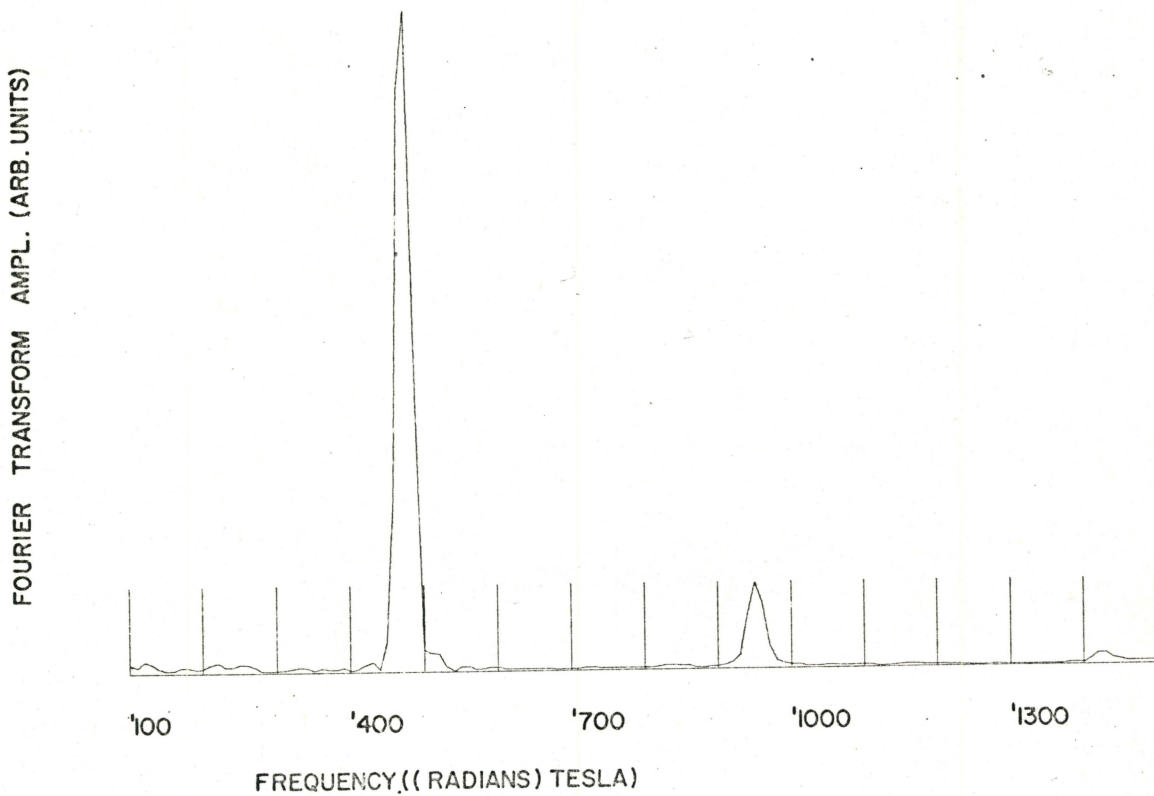
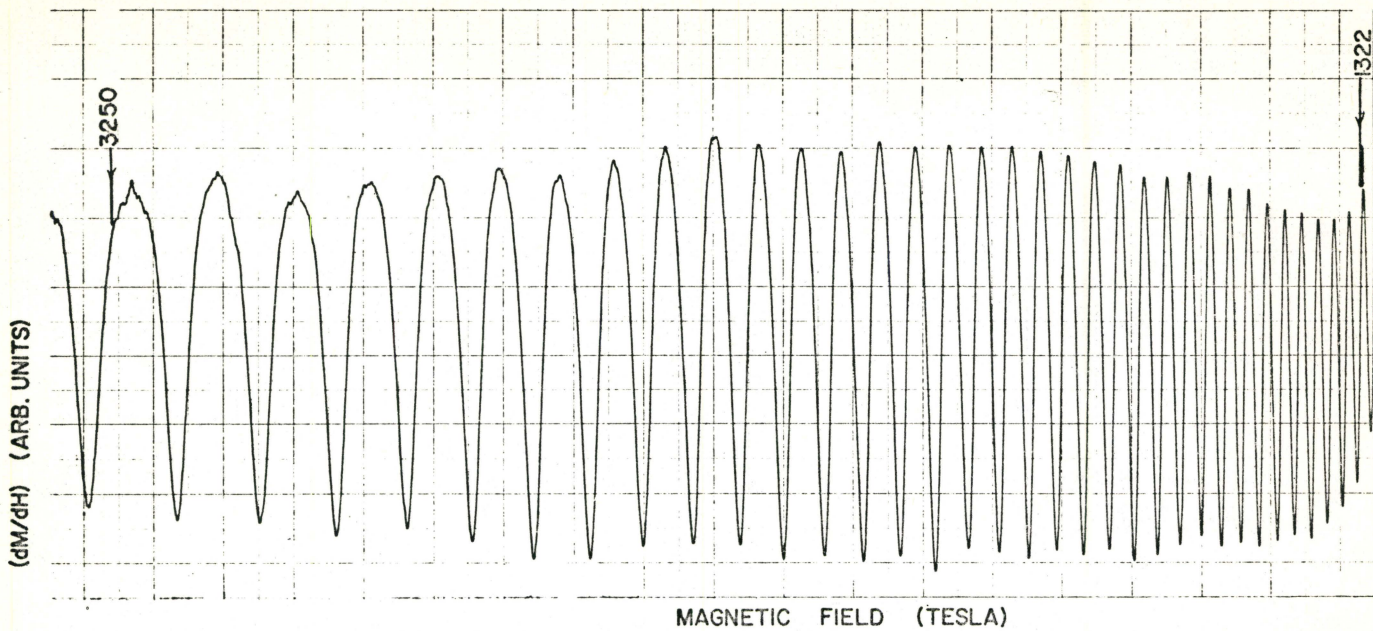


Fig. (V.1)

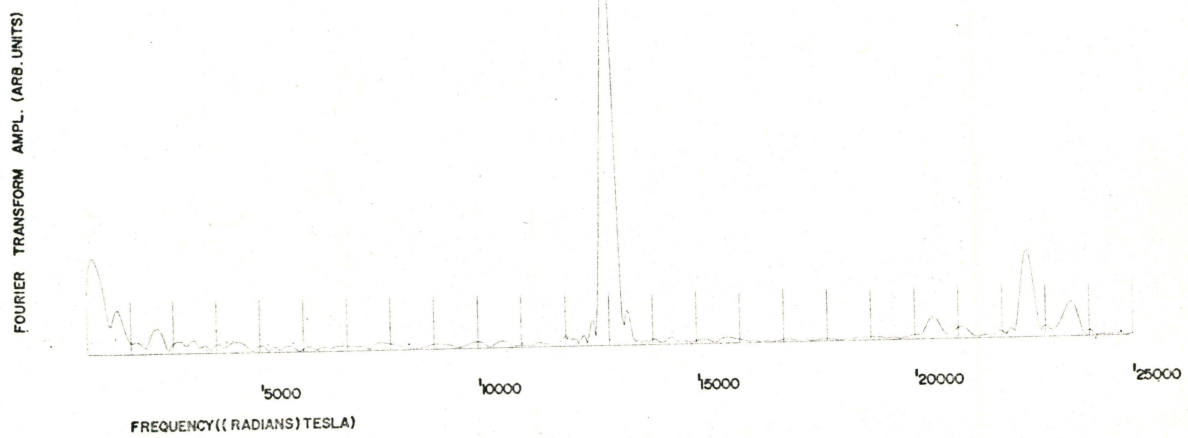
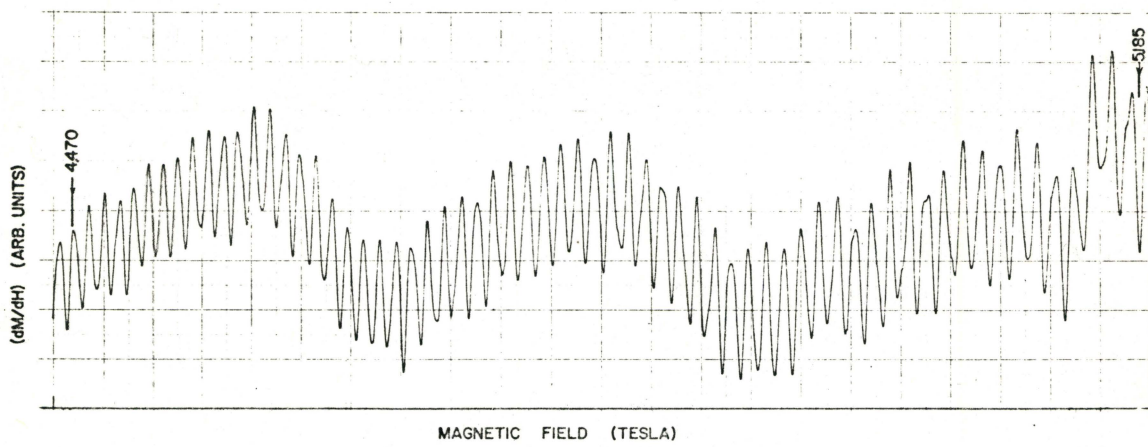
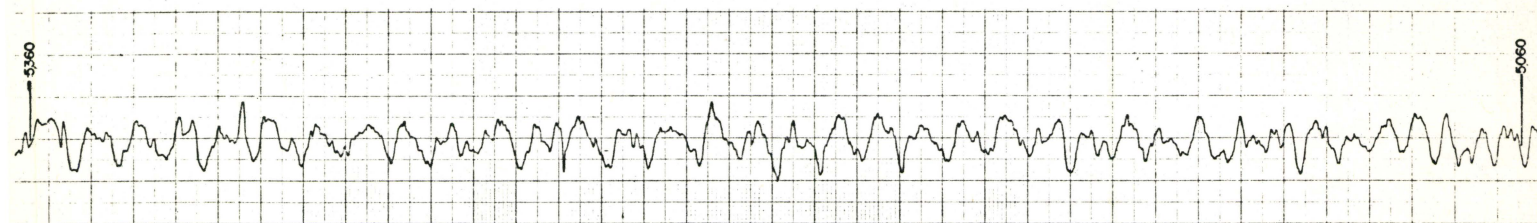


Fig. (V.2)



MAGNETIC FIELD (TESLA)

FOURIER TRANSFORM AMPL. (ARB. UNITS)

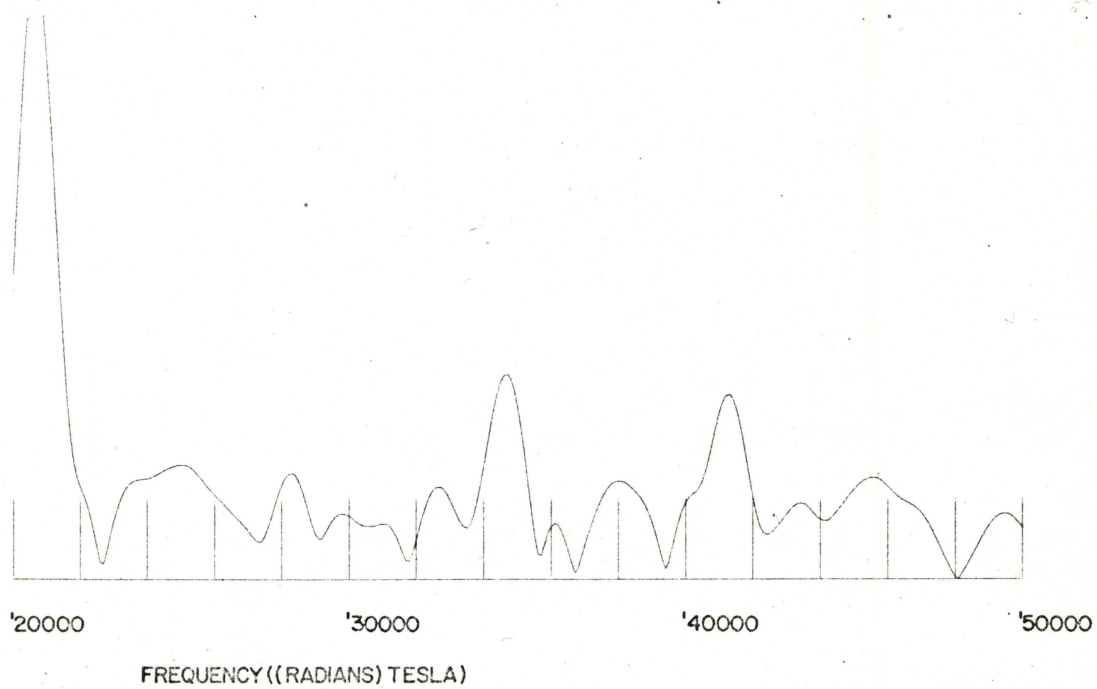


Fig. (V.3)

BIBLIOGRAPHY

1. W. J. de Haas and P. M. van Alphen, Leiden Comm, 208d, 212a, (1930) and 220d (1932).
2. L. D. Landau, Z. Phys. 64, 629, 1930.
3. R. Peierls, Z. Phys., 81, (1933).
4. L. Onsager, Phil. Mag. 43, 1006 (1952).
5. I. M. Lifshitz and A. M. Kosevich, J. Exp. Th. Phys., U.S.S.R., 29, 730, (1955).
6. A. B. Pippard, Lecture Notes Simon Fraser Summer School, 1967.
7. A.B. Pippard, Lecture notes Simon Fraser Summer School, 1967.
8. R.B. Dingle, Proc. Roy.Soc., A.211, 500 (1952).
9. R.B. Dingle, Proc. Roy. Soc., A.211, 517 (1952).
10. A. E. Dixon (Thesis, McMaster University 1966).